Cell

Ferroptosis surveillance independent of GPX4 and differentially regulated by sex hormones

Graphical abstract

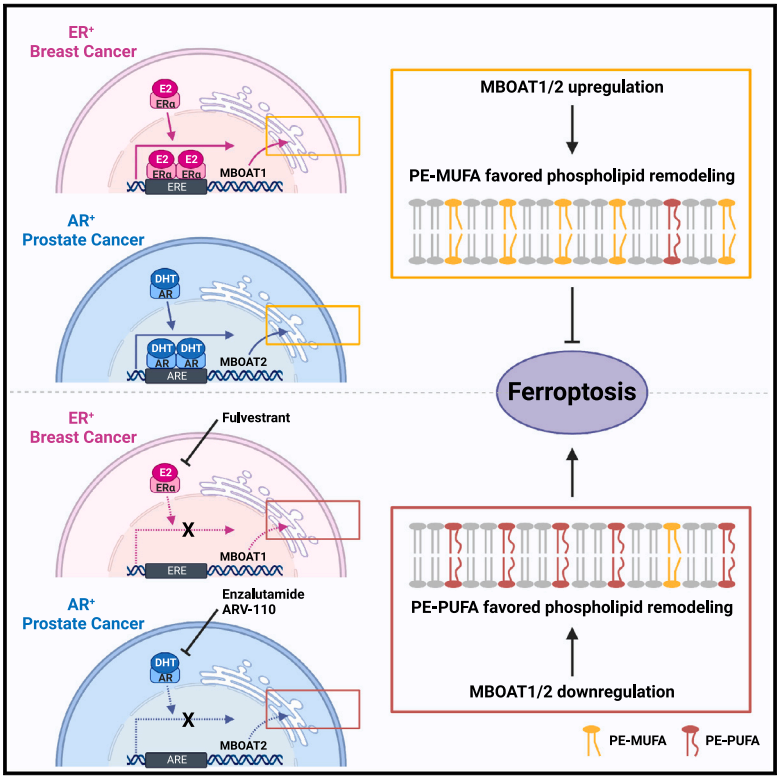

Highlights

- MBOAT1/2 suppress ferroptosis through phospholipid remodeling independently of GPX4
- MBOAT1 and MBOAT2 are regulated by ER and AR signaling, respectively
- ER antagonists sensitize ER$^+$ breast cancer to ferroptosis by downregulating MBOAT1
- AR antagonists sensitize AR$^+$ prostate cancer to ferroptosis by downregulating MBOAT2

Authors

Deguang Liang, Yan Feng, Fereshteh Zandkarimi, ..., Wei Gu, Brent R. Stockwell, Xuejun Jiang

Correspondence

jiangx@mskcc.org

In brief

MBOAT1 and MBOAT2 are sex hormone-dependent ferroptosis regulators with therapeutic implications for ER$^+$ breast cancer and AR$^+$ prostate cancer, respectively.

Liang et al., 2023, Cell *186*, 1–17
June 22, 2023
https://doi.org/10.1016/j.cell.2023.05.003

CellPress

Please cite this article in press as: Liang et al., Ferroptosis surveillance independent of GPX4 and differentially regulated by sex hormones, Cell (2023), https://doi.org/10.1016/j.cell.2023.05.003

Cell

CellPress

Article

Ferroptosis surveillance independent of GPX4 and differentially regulated by sex hormones

Deguang Liang,[1] Yan Feng,[1] Fereshteh Zandkarimi,[2] Hua Wang,[1] Zeda Zhang,[3] Jinnie Kim,[1] Yanyan Cai,[4] Wei Gu,[5] Brent R. Stockwell,[2] and Xuejun Jiang[1,6,*]

[1]Cell Biology Program, Memorial Sloan Kettering Cancer Center, New York, NY 10065, USA
[2]Department of Biological Sciences, Department of Chemistry, Columbia University, New York, NY 10027, USA
[3]Cancer Biology and Genetics Program, Memorial Sloan Kettering Cancer Center, New York, NY 10065, USA
[4]Human Oncology and Pathogenesis Program, Memorial Sloan Kettering Cancer Center, New York, NY 10065, USA
[5]Herbert Irving Comprehensive Cancer Center, Columbia University, New York, NY 10032, USA
[6]Lead contact
*Correspondence: jiangx@mskcc.org
https://doi.org/10.1016/j.cell.2023.05.003

SUMMARY

Ferroptosis, a cell death process driven by iron-dependent phospholipid peroxidation, has been implicated in various diseases. There are two major surveillance mechanisms to suppress ferroptosis: one mediated by glutathione peroxidase 4 (GPX4) that catalyzes the reduction of phospholipid peroxides and the other mediated by enzymes, such as FSP1, that produce metabolites with free radical-trapping antioxidant activity. In this study, through a whole-genome CRISPR activation screen, followed by mechanistic investigation, we identified phospholipid-modifying enzymes MBOAT1 and MBOAT2 as ferroptosis suppressors. MBOAT1/2 inhibit ferroptosis by remodeling the cellular phospholipid profile, and strikingly, their ferroptosis surveillance function is independent of GPX4 or FSP1. MBOAT1 and MBOAT2 are transcriptionally upregulated by sex hormone receptors, i.e., estrogen receptor (ER) and androgen receptor (AR), respectively. A combination of ER or AR antagonist with ferroptosis induction significantly inhibited the growth of ER^+ breast cancer and AR^+ prostate cancer, even when tumors were resistant to single-agent hormonal therapies.

INTRODUCTION

As a specific form of regulated cell death, ferroptosis plays crucial roles in multiple pathological conditions including cancer, ischemic organ injuries, and degenerative diseases; increasing evidence also implicates potential physiological functions of ferroptosis.[1–3] Ferroptosis is executed by iron-dependent phospholipid (PL) peroxidation, leading to plasma membrane rupture and eventual cell death. As PL peroxidation is a natural outcome of normal cellular metabolism and various stresses frequently encountered by the cell, surveillance mechanisms are required to prevent unwanted ferroptosis. There are two major ferroptosis surveillance mechanisms: one is mediated by glutathione (GSH) peroxidase 4 (GPX4)—the sole mammalian enzyme known to reduce PL peroxides (PLOOH) to corresponding PL alcohols—which sets GPX4 and its upstream cyst(e)ine import and GSH synthesis as the primary mechanism to suppress ferroptosis[4,5]; the other is mediated by enzymes such as FSP1, DHODH, NOS2, and GCH1 that produce metabolites with radical-trapping antioxidant (RTA) activity,[6–11] thus terminating PL peroxidation—the prerequisite of ferroptosis.

Mounting evidence suggests ferroptosis as an innate tumor suppressive mechanism mediating the anticancer activity of multiple tumor suppressors[12–14] and ferroptosis induction as a potential cancer therapeutic approach to selectively eliminate cancer cells of specific genetic backgrounds, either as a single-agent therapy or in combination with other targeted agents, including PI3K/mTOR pathway inhibitors and immune checkpoint blockades.[15–20] Although controversies exist on how tumor cell ferroptosis may engage or dampen antitumor immunity,[21,22] multiple studies using immune-competent mice have unambiguously demonstrated the anticancer effect of ferroptosis induction for tumors of specific genetic background.[18,20,23] Therefore, understanding mechanisms of ferroptosis holds value for both basic biology and disease treatment. It is particularly important to determine whether there exist additional surveillance mechanisms independent of GPX4 and RTAs—cancer cells may exploit such new mechanisms to evade ferroptosis, and conversely, these mechanisms can shed light on the development of novel combination therapies.

In this study, we utilized a whole-genome CRISPR activation screen and identified membrane bound O-acyltransferase domain containing 2 (MBOAT2), a lyso-PL acyltransferase (LPLAT), as a ferroptosis-suppressing gene. We demonstrate that MBOAT2 selectively transfers monounsaturated fatty acids (MUFAs) into lyso-phosphatidylethanolamine (lyso-PE), hence increasing cellular PE-MUFA and correspondingly decreasing cellular PE-PUFA (polyunsaturated fatty acid). Since PE-PUFA

Please cite this article in press as: Liang et al., Ferroptosis surveillance independent of GPX4 and differentially regulated by sex hormones, Cell (2023), https://doi.org/10.1016/j.cell.2023.05.003

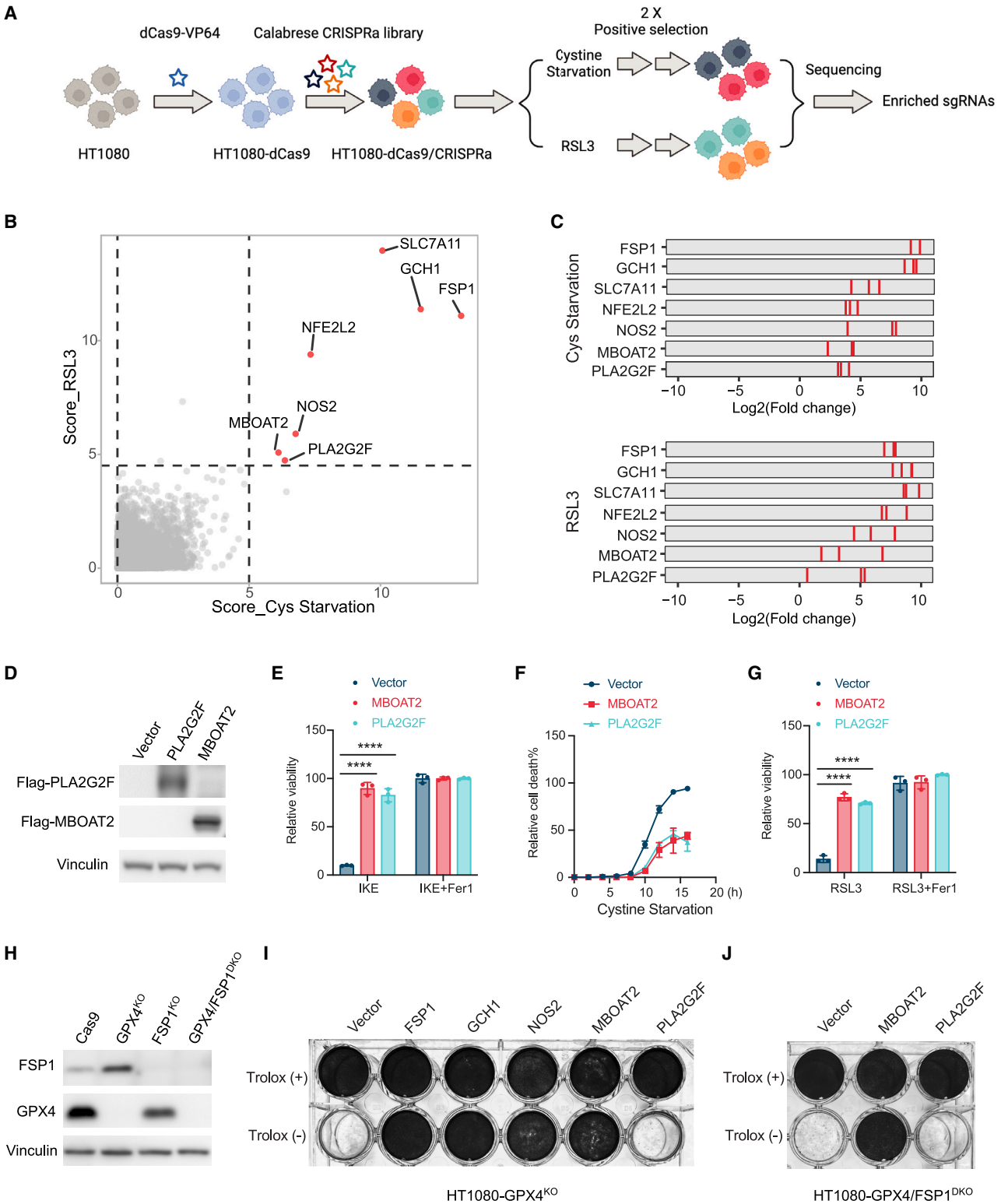

Figure 1. MBOAT2 is a GPX4/FSP1-independent ferroptosis suppressor

(A) Schematic plot summarizing the workflow of CRISPR activation screen in HT1080 cells.

(B) Top seven genes enriched in both RSL3 and cystine starvation conditions are highlighted.

(C) Visualization of enrichment for sgRNAs targeting top seven genes in cystine starvation (top) and RSL3 (bottom) screen conditions.

(legend continued on next page)

Please cite this article in press as: Liang et al., Ferroptosis surveillance independent of GPX4 and differentially regulated by sex hormones, Cell (2023), https://doi.org/10.1016/j.cell.2023.05.003

is the preferred substrate for PL peroxidation and a major determinant of ferroptosis sensitivity,[24,25] MBOAT2 can potently inhibit ferroptosis. More importantly, MBOAT2 can prevent ferroptosis independently of GPX4 and FSP1 through a PL remodeling-mediated surveillance mechanism. We also show that another LPLAT member, MBOAT1, suppresses ferroptosis via similar mechanism. Strikingly, MBOAT2 and MBOAT1 are directly upregulated by androgen receptor (AR) and estrogen receptor (ER), respectively. Anti-AR drugs enzalutamide (ENZ) and ARV-110 sensitized AR^+ prostate cancer (PCa) cells to ferroptosis by downregulating MBOAT2 expression, and ER degrader fulvestrant (Ful) sensitized ER^+ breast cancer (BCa) cells to ferroptosis through downregulating MBOAT1. Collectively, we demonstrate that sex hormone signaling restrains cancer cells from ferroptosis through MBOAT1/2-mediated PL remodeling, and these regulatory events can be explored for the treatment of cancers with specific genetic background.

RESULTS

MBOAT2 is a ferroptosis suppressor independent of GPX4 and FSP1

To identify ferroptosis-suppressing genes, we conducted a genome-wide CRISPR activation screen in human fibrosarcoma HT1080 cells, with GPX4 inhibitor RSL3 and cystine starvation as ferroptosis inducers (FINs) (Figure 1A). sgRNAs of 7 genes were found to be most enriched in cells that survived both RSL3 and cystine starvation (Figures 1B and 1C). Among them, 5 are established ferroptosis suppressors: SLC7A11, NFE2L2/NRF2, FSP1, GCH1, and NOS2; the other two are lipid modifying enzymes MBOAT2 and PLA2G2F, which have not been reported as ferroptosis regulators.

As a member of the membrane bound O-acyltransferase (MBOAT) family, MBOAT2 possesses LPLAT activity, preferentially transferring MUFAs to the Sn2 position of lyso-PE and likely also to lyso-phosphatidylcholine (PC) and lyso-phosphatidic acid (PA).[26,27] PLA2G2F (group IIF secretory phospholipase A2) is a calcium-dependent PLA2.[28] Both MBOAT2 and PLA2G2F are presumably involved in the PL remodeling pathway, Lands' cycle—to de-acylate PLs by phospholipase A1/2 (PLA1/2) and acylate lyso-PL by LPLATs—through which fatty acyl side chains of PLs are selectively replaced.[29] Because the composition of plasma membrane PL determines ferroptosis sensitivity, enzymatic components of Lands' cycle are potential regulators of ferroptosis.[30] Indeed LPCAT3 (MBOAT5), another member of the MBOAT family, promotes ferroptosis by incorporating PUFAs into PLs to increase the level of PL-PUFAs, the substrate of PL peroxidation.[31] Interestingly, iPLA2β, a member of the PLA2 family, has been reported to negatively regulate ferroptosis, possibly by removing oxidized acyl chains of PLs.[32–34]

To validate whether MBOAT2 and PLA2G2F possess a ferroptosis-suppressing function, we overexpressed them in HT1080 cells (Figure 1D) and found that both inhibited ferroptosis induced by imidazole ketone erastin (IKE), an inhibitor of cystine/glutamate antiporter system x_c^-, and by cystine starvation (Figures 1E and 1F). These inducers, known as class I FINs, trigger ferroptosis by depleting GPX4 cofactor GSH. Overexpression of MBOAT2 and PLA2G2F also inhibited ferroptosis induced by RSL3, a direct inhibitor of GPX4, a class II FIN (Figure 1G). Next, we established HT1080-$GPX4^{KO}$ cells as a spontaneous ferroptosis model (Figure 1H). These cells are maintained in the presence of antioxidant trolox to prevent ferroptosis. After removal of trolox, HT1080-$GPX4^{KO}$ cells undergo ferroptosis promptly (Figure S1A). Strikingly, MBOAT2 overexpression, but not PLA2G2F, enabled the maintenance of long-term culture of HT1080-$GPX4^{KO}$ cells without trolox, reminiscent of the GPX4-independent anti-ferroptosis function of RTA-generating enzymes FSP1, GCH1, and NOS2 (Figures 1I and S1B–S1D). We observed that FSP1 is upregulated in HT1080-$GPX4^{KO}$ cells, likely through feedback regulation (Figure 1H). We thus established HT1080-GPX4/$FSP1^{DKO}$ cells (Figures 1H and S1A) and found that MBOAT2 effectively rescued spontaneous ferroptosis and maintained long-term viability of GPX4/$FSP1^{DKO}$ cells (Figure 1J). Consistently, MBOAT2 inhibited RSL3-induced lipid peroxidation, a critical event for ferroptosis (Figure S1E). In summary, MBOAT2 is a potent ferroptosis-suppressing gene that functions independently of GPX4 activity and FSP1. Notably, RNA-seq analysis revealed that MBOAT2 overexpression did not alter the expression of other known ferroptosis regulators (Figures S1F and S1G; Table S1).

Ferroptosis suppression by MBOAT2 requires either endogenous or exogenous MUFA

We subsequently tested whether MBOAT2 suppresses ferroptosis through PL metabolism. MBOAT2 exhibits LPLAT activity by transferring oleic acid (OA; 18:1), in its CoA-conjugated acyl donor form, to lyso-PE and likely also to lyso-PC and lyso-PA.[26,27] With OA as one of the most abundant cellular MUFAs, and both endogenous MUFA synthesis through SCD1 and exogenous MUFAs able to suppress ferroptosis in an ACSL3-dependent manner,[16,35] we hypothesize that MBOAT2 catalyzes MUFA incorporation into PL, competitively decreasing PL-PUFA content and ultimately leading to a ferroptosis-resistant cell state. This hypothesis predicts that either endogenous MUFA synthesis or exogenous MUFAs can mediate the ferroptosis-suppressing activity of MBOAT2.

We conducted the following experiments to test the role of endogenous MUFA synthesis. *De novo* lipogenesis of MUFAs

(D) Western blot confirming overexpression of MBOAT2 and PLA2G2F in HT1080 cells.
(E and G) Viability analysis of HT1080 cells overexpressing indicated genes. Cells were treated with 0.3 μM IKE (E) or 0.1 μM RSL3 (G) for 24 h, in the absence or presence of ferrostastin-1 (Fer1, 10 μM).
(F) Cell death time course of HT1080 cells overexpressing indicated genes. Ferroptosis was induced by cystine starvation.
(H) Western blot confirming knockout of GPX4 and/or FSP1 in HT1080 cells.
(I and J) Crystal violet staining of HT1080-$GPX4^{KO}$ cells (I) or HT1080-GPX4/$FSP1^{DKO}$ cells (J) overexpressing indicated genes cultured with or without trolox for 72 h. Two independent experiments were performed, and representative images from one experiment are shown.
Data are presented as mean ± SD, n = 3 biologically independent samples in (E) and (G). Statistical analysis was performed using one-way ANOVA. *$p < 0.05$, **$p < 0.01$, ***$p < 0.001$, and ****$p < 0.0001$ (p value classification applies to all later figures).
See also Figure S1.

Please cite this article in press as: Liang et al., Ferroptosis surveillance independent of GPX4 and differentially regulated by sex hormones, Cell (2023), https://doi.org/10.1016/j.cell.2023.05.003

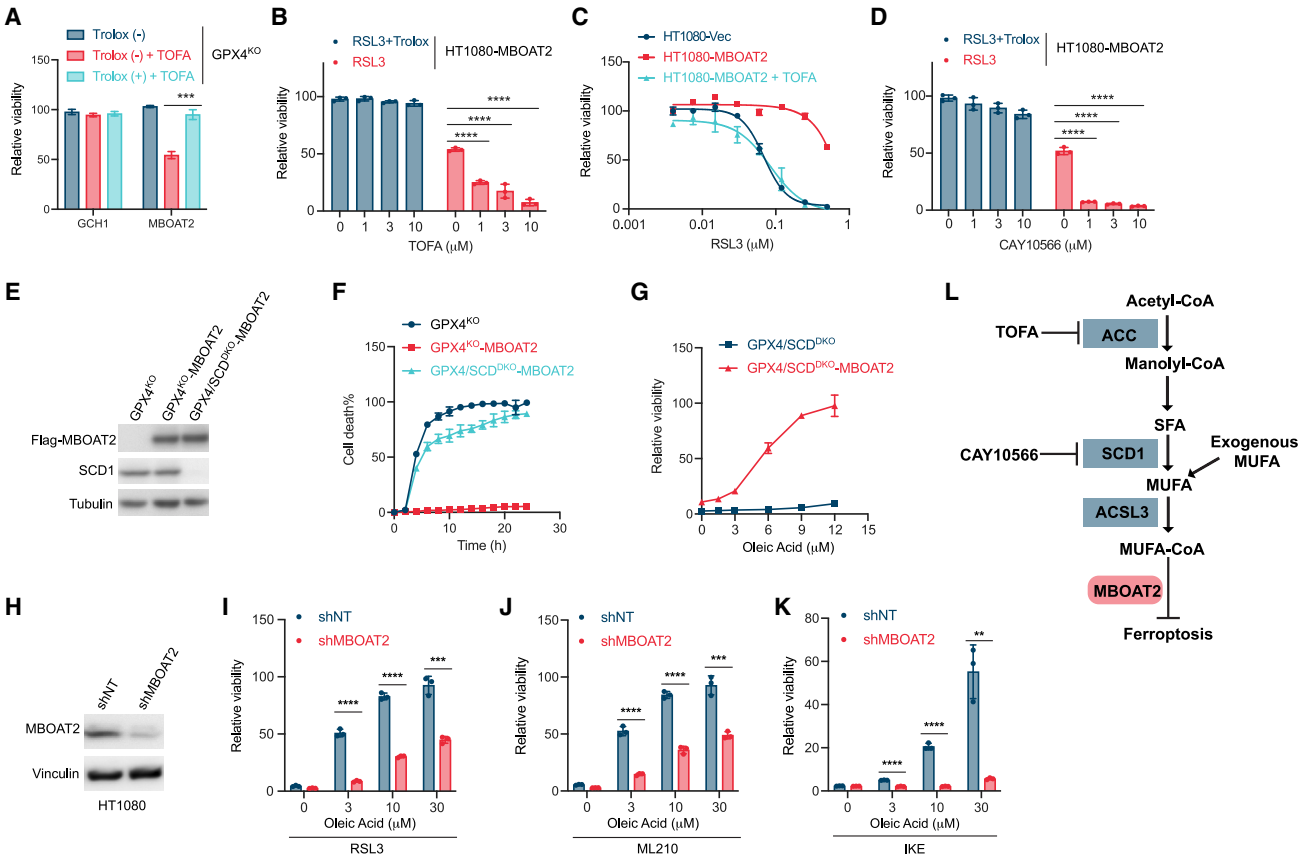

Figure 2. The ferroptosis-suppressing function of MBOAT2 requires either endogenous or exogenous MUFA

(A) Viability analysis of HT1080-GPX4^{KO} cells overexpressing GCH1 or MBOAT2. Cells were treated for 48 h with TOFA (5 μM) in the presence or absence of trolox (100 μM), as indicated.

(B and D) Viability analysis of HT1080-MBOAT2 cells. Cells were pretreated with indicated concentration of TOFA (B) or CAY10566 (D) for 24 h, followed by ferroptosis induction with RSL3 (0.1 μM) in the presence or absence of trolox for another 24 h.

(C) Viability assay of HT1080-vector and HT1080-MBOAT2 cells. Cells were pretreated with or without TOFA (5 μM) as indicated for 24 h, followed by indicated concentrations of RSL3 for another 24 h.

(E) Western blot analysis showing expression of SCD1 and MBOAT2 in indicated HT1080 cells.

(F) Cell death time course of cells with indicated genetic background and with or without MBOAT2 overexpression. Cells were originally cultured in the presence of trolox, and ferroptosis was initiated by removing trolox (that was the starting point of the time course).

(G) Viability analysis of HT1080-GPX4/SCD^{DKO} cells with or without MBOAT2 overexpression as indicated. Cells were pretreated with indicated concentration of oleic acid (OA) plus trolox for 16 h, and ferroptosis was induced by removing trolox but keeping same amount of OA, for another 24 h.

(H) Western blot analysis confirming knockdown of MBOAT2 in HT1080 cells.

(I–K) Viability analysis of HT1080 cells with control or MBOAT2 shRNA. Cells were pretreated with indicated concentration of OA for 16 h and followed by ferroptosis induction with 0.1 μM RSL (I), 1 μM ML210 (J), or 0.5 μM IKE (K) for 24 h.

(L) Working model showing MBOAT2 utilizes endogenous or exogenous MUFA to suppress ferroptosis.

Data are presented as mean ± SD, n = 3 biologically independent samples in (A)–(D), (F), (G), and (I)–(K).

Statistical analysis was performed using one-way ANOVA in (B) and (D) or two-tailed t test in (A) and (I)–(K). See also Figure S2.

starts with carboxylation of acetyl-CoA to form malonyl-CoA by acetyl-CoA carboxylase (ACC). ACC inhibitor TOFA induced ferroptosis in HT1080-GPX4^{KO} cells with MBOAT2 overexpression in a dose-dependent manner (Figure S2A), but not in HT1080-GPX4^{KO} cells with GCH1 overexpression (Figure 2A), suggesting a MBOAT2-specific role of lipogenesis in ferroptosis suppression. Consistently, TOFA potentiated RSL3-induced ferroptosis in HT1080 cells overexpressing MBOAT2 in a dose-dependent manner (Figure 2B) and could completely abolish the ferroptosis-suppressing activity of MBOAT2 (Figure 2C). *De novo* synthesized saturated fatty acids (SFAs) are converted to MUFAs by SCD1, hence we tested whether SCD1 is required for the ferroptosis-suppressing function of MBOAT2. Indeed, SCD1 inhibitor CAY10566 ablated the protective activity of MBOAT2 against ferroptosis induced by RSL3 or GPX4 knockout (Figures 2D and S2B). SCD1 knockout confirmed the effect of CAY-10566 (Figures 2E and 2F). Collectively, these results confirmed the role of *de novo* MUFA synthesis in mediating the ferroptosis-suppressing function of MBOAT2. Further, ACSL3 selectively converts MUFAs into MUFA-CoA before their incorporation into PL, which is required for the ferroptosis-suppressing function of MUFA.[35] In agreement with this, ACSL3 knockdown provoked

Please cite this article in press as: Liang et al., Ferroptosis surveillance independent of GPX4 and differentially regulated by sex hormones, Cell (2023), https://doi.org/10.1016/j.cell.2023.05.003

CellPress

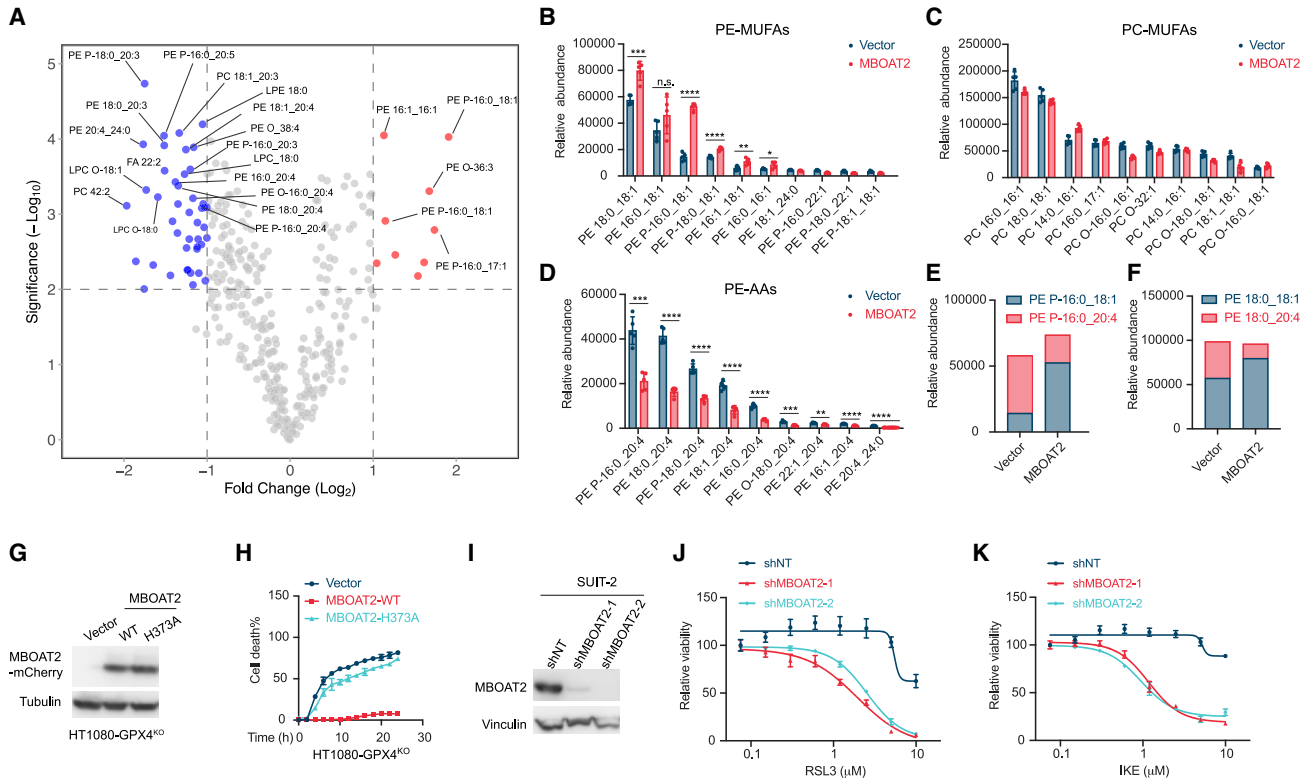

Figure 3. MBOAT2 suppresses ferroptosis through phospholipid remodeling

(A) Volcano plot showing upregulated lipid species (red) and downregulated lipid species (blue) by MBOAT2 overexpression in HT1080 cells. Cutoff: FC threshold = 2, $p < 0.01$; two-tailed t test. See also Table S2.

(B–D) Quantification of most abundant PE-MUFAs (B), PC-MUFAs (C), and PE-AAs (D) in HT1080-vector and HT1080-MBOAT2 cells, as indicated.

(E and F) Stacked bars showing relative abundance of indicated PE-OA and PE-AA in HT1080-vector and HT1080-MBOAT2 cells.

(G) Western blot showing the expression of MBOAT2 wild-type (WT) and H373A mutant in HT1080-GPX4^{KO} cells.

(H) Cell death time course of HT1080-GPX4^{KO} cells overexpressing MBOAT2 WT or H373A mutant, as indicated. Ferroptosis was initiated by removing trolox from culture medium.

(I) Western blot showing MBOAT2 knockdown in SUIT-2 cells.

(J and K) Viability analysis of SUIT-2 cells expressing control or MBOAT2 shRNA. Ferroptosis was induced by indicated concentration of RSL3 for 24 h.

Data are presented as mean ± SD, n = 5 biologically independent samples in (B)–(D) or n = 3 biologically independent samples in (H), (J), and (K). Statistical analysis was performed using two-tailed t test in (B)–(D).

See also Figure S3.

spontaneous ferroptosis in HT1080-GPX4^{KO} cells, even with MBOAT2 overexpression (Figures S2C and S2D).

In addition to *de novo* synthesis, dietary FA is also an important source of MUFA pool. Indeed, exogenous OA attenuated ferroptosis in HT1080-GPX4^{KO} cells (Figure S2E). Upon MBOAT2 overexpression, the protective function of OA was further increased in HT1080-GPX4/SCD1^{DKO} cells (Figure 2G), whereas MBOAT2 knockdown significantly diminished protection conferred by exogenous OA (Figures 2H–2K). In conclusion, MBOAT2 mediates the ferroptosis-suppressing activity of both endogenous and exogenous MUFAs (see working model in Figure 2L).

MBOAT2 suppresses ferroptosis through phospholipid remodeling

As MBOAT2 suppresses ferroptosis in a MUFA-dependent manner, we sought to determine whether MBOAT2 inhibits ferroptosis through PL remodeling. We performed untargeted lipidomic analysis in HT1080 cells with or without MBOAT2 overexpression. In total, we have measured the relative abundance of 370 lipid species (Table S2). PE-PUFAs are significantly downregulated by MBOAT2 overexpression, while PE-MUFAs are clustered among the top upregulated lipids in MBOAT2-overexpression cells (Figure 3A). Previous studies suggest that PEs with arachidonoyl tail (PE-AA, 20:4) or adrenoyl tail (PE-AdA, 22:4) are the major PL-PUFAs that are subjected to peroxidation during ferroptosis.[24,25] Since MBOAT2 mainly affects PE lipids, we propose that MBOAT2 selectively transfers MUFA-CoA to lyso-PE to competitively decrease the incorporation of PUFA-CoA into lyso-PE. To test this possibility, we reexamined alteration by MBOAT2 overexpression of major PE-MUFAs, PC-MUFAs, as well as other PL-MUFAs (ranked by relative abundance). Compared with control, overexpression of MBOAT2 selectively increased PE-MUFAs, especially PE-OAs (18:1); however, PC-MUFAs and other PL-MUFAs were not significantly affected

Please cite this article in press as: Liang et al., Ferroptosis surveillance independent of GPX4 and differentially regulated by sex hormones, Cell (2023), https://doi.org/10.1016/j.cell.2023.05.003

(Figures 3B, 3C, and S3A). We noticed that ester linkage PE-MUFAs (e.g., PE 18:0_18:1) and ether linkage PE-MUFAs (e.g., PE P-18:0_18:1) increased in a similar trend (Figure 3B), suggesting that the chemistry of sn-1 linkage does not affect the activity of MBOAT2.

Next, we examined how MBOAT2 regulates the PE-PUFA profile. PE-PUFAs were significantly decreased upon MBOAT2 overexpression (Figure 3D), while most of other PL-PUFAs were not affected (Figures S3B and S3C). Interestingly, among PE-PUFAs, PE-AAs were significantly decreased (Figure 3D); again, both ester linkage PE-AAs (e.g., PE 18:0/20:4) and ether linkage PE-AAs (e.g., PE 18:0/20:4) were similarly decreased (Figure 3D). However, PE-AdAs and other PE-long-chain PUFAs (e.g., 22:4, 22:5, 22:6) were not significantly affected (Figure S3D). Considering that AA releases from PL much faster than AdA,[36] PE-AA might be subject to more active PL remodeling, which explains why PE-AA but not PE-AdA was altered by MBOAT2. Collectively, our data support a competitive PE remodeling model, in which MUFA-preferred lyso-PE acyltransferase (LPEAT) MBOAT2 competes with PUFA-preferred LPEAT (e.g., LPCAT3) on lyso-PE. Presumably, in specific cells or tissues with predominant MBOAT2 activity, PE remodeling would shift the cells toward a state of high PE-MUFA level but low PE-PUFA level, leading to ferroptosis resistance, and vice versa (Figure S3E). In agreement with this competition model, we found that the increase of PE-OAs was very similar to the decrease of PE-AAs that share the same backbone of lyso-PE (e.g., PE 18:0_18:1 vs. PE 18:0_20:4; Figures 3E and 3F). Furthermore, mutation of MBOAT2 enzymatic site H373 completely abolished its ferroptosis-suppressing function (Figures 3G and 3H), validating that the enzymatic activity of MBOAT2 is essential for ferroptosis inhibition.

The function of MBOAT2 to inhibit ferroptosis is not limited to HT1080 cells. Through an analysis of DepMap portal, we found that *MBOAT2* mRNA expression was positively correlated with RSL3 resistance in pancreatic ductal adenocarcinoma (PDAC) cells (Figure S3F). Indeed, in a panel of PDAC cells, we confirmed that MBOAT2-mid/high cells generally showed more resistance to RSL3, compared with MBOAT2-low cells (Figures S3G and S3H). Moreover, overexpressing MBOAT2 in MBOAT2-low PANC-1 and MIA PaCa-2 cells significantly increased their resistance to ferroptosis induction (Figures S3I–S3L), whereas knocking down MBOAT2 in SUIT-2 cells sensitized cells to ferroptosis (Figures 3I–3K).

Mammalian cells acquire essential PUFAs, α-linolenic acid (ALA; 18:3n-3) and linoleic acid (LA; 18:2n-6), through diet and further synthesize other long-chain PUFAs (e.g., AA) through a chain of desaturation and elongation reactions.[30] In the context of tumor microenvironment, CD36-mediated fatty acid uptake increases PL-PUFA contents and promotes ferroptosis in tumor-infiltrating $CD8^+$ T cells.[37] Since MBOAT2 competitively inhibits synthesis of PE-PUFAs, we sought to examine whether MBOAT2 is responsible for the resistance of exogenous PUFA-induced ferroptosis. Exogenous PUFA (LA) sensitized RSL3- or IKE-induced ferroptosis in SUIT-2 cells, and this sensitization was significantly amplified by MBOAT2 knockdown (Figures S3M and 3N), indicating that endogenous MBOAT2 plays a significant role in antagonizing exogenous PUFA-induced ferroptosis.

Androgen receptor (AR) signaling modulates ferroptosis in prostate cancer through MBOAT2

Through a cross comparison of *MBOAT2* mRNA levels in various cancer tissues (TCGA PanCancer Atlas) as well as in normal tissues (GTEx Portal), we found that MBOAT2 is frequently upregulated in prostate cancer (PCa) (Figures 4A and S4A). Intriguingly, *MBOAT2* mRNA is positively correlated with *AR* mRNA in human PCa samples (Figure S4B; TCGA PanCancer Atlas). By analyzing a panel of PCa cell lines, we confirmed that MBOAT2 was highly expressed in AR^+ PCa cell lines but not in AR^- PCa cell lines (Figure 4B). Importantly, AR^+ PCa cell lines were generally more resistant to ferroptosis than AR^- PCa cell lines (Figure 4C). These results prompted us to propose that AR signaling modulates ferroptosis in PCa through MBOAT2.

Our analysis of previously published ChIP-seq dataset (GSE37345)[38] revealed that AR and its cofactor FOXA1 bind to a putative intronic androgen response element (ARE) with proximity to the transcription start site (TSS) of *MBOAT2* (Figure 4D). Through a ChIP-qPCR analysis, we confirmed the binding of AR to this *MBOAT2* ARE and that this binding was enhanced by AR agonist dihydrotestosterone (DHT) but inhibited by AR antagonist ENZ (Figure 4E). Further, DHT stimulated MBOAT2 expression in AR^+ PCa cell lines (Figures 4F and S4C), while ENZ decreased baseline MBOAT2 expression (Figure 4B) and abolished DHT-induced MBOAT2 upregulation (Figures 4F, S4C, and S4D). As expected, inducible shRNA knockdown of AR decreased MBOAT2 expression in LnAR cells (LNCaP cells with AR overexpression) (Figure 4G), and ectopic expression of AR in AR^- PC3 cell line induced MBOAT2 expression that was further increased by DHT (Figure 4H). Moreover, knockdown of FOXA1 decreased MBOAT2 gene expression in LnAR cells (Figure S4E). Collectively, MBOAT2 is a *bona fide* target of AR in PCa cells.

We next examined whether AR regulates MBOAT2 expression in normal prostate tissues. An analysis of single-cell RNA-seq datasets[39] showed that *MBOAT2* expression in normal human prostate tissues decreased after androgen deprivation therapy (ADT) (Figure S4F), and *Mboat2* expression in normal mouse prostate tissues diminished after castration and restored rapidly after androgen addback (Figure S4G). Further, in mouse normal prostate organoids, Mboat2 was downregulated by ENZ (Figure S4H) and upregulated by DHT and AR overexpression (Figure S4I). Therefore, AR signaling regulates MBOAT2 expression in both normal prostate tissues and PCa.

We subsequently examined whether MBOAT2 regulates ferroptosis sensitivity in AR^+ PCa. MBOAT2 knockout or knockdown significantly sensitized LnAR (Figures 4I–4J, S4J, and S4K) and LNCaP cells (Figures S4L and S4M) to RSL3-induced ferroptosis. Through lipidomic analysis (Figure S4N; Table S3), we found that MBOAT2 knockdown remodeled PL profile by significantly increasing the contents of PE-PUFAs (Figure 4K) but decreasing that of selected PE-MUFAs (Figure 4L). Therefore, AR signaling promotes the resistance of AR^+ PCa cells to ferroptosis via upregulating MBOAT2 expression and subsequently remodeling cellular PL profile.

Please cite this article in press as: Liang et al., Ferroptosis surveillance independent of GPX4 and differentially regulated by sex hormones, Cell (2023), https://doi.org/10.1016/j.cell.2023.05.003

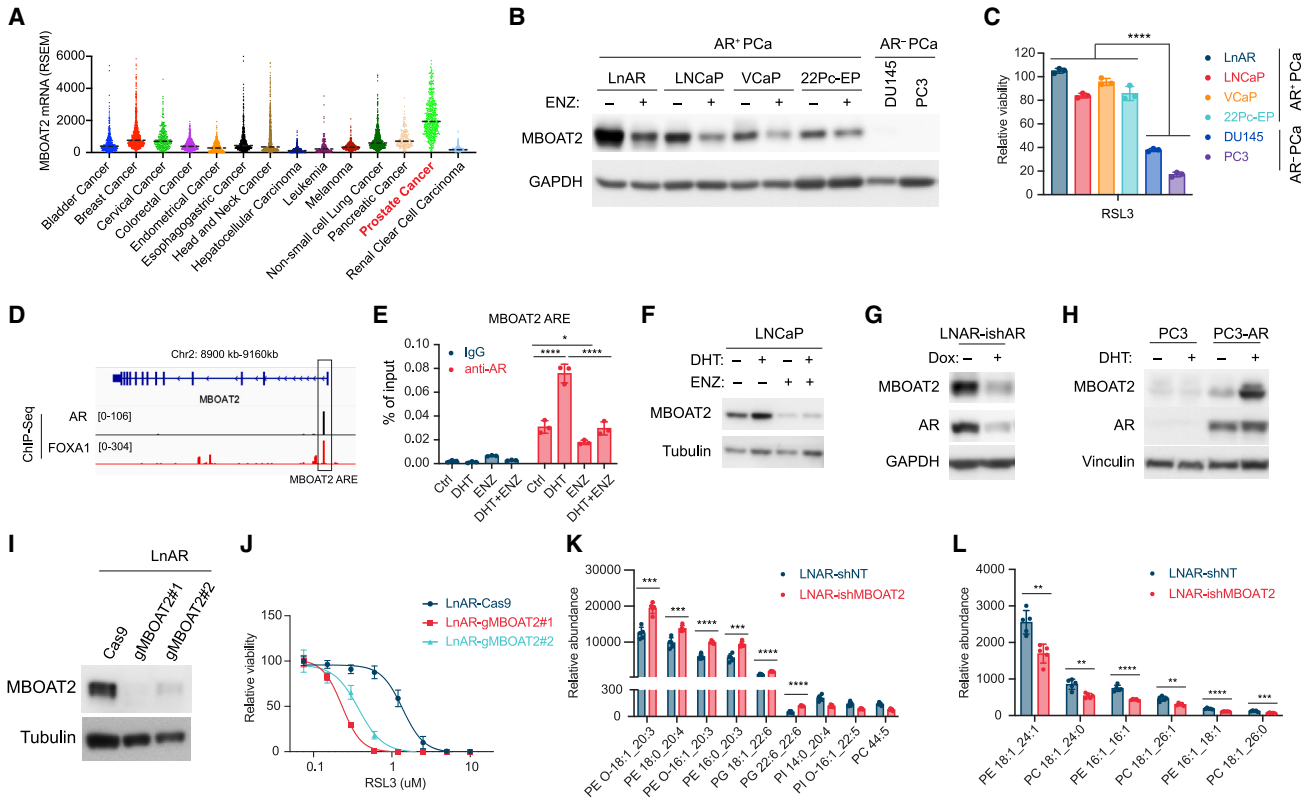

Figure 4. AR signaling modulates ferroptosis sensitivity in prostate cancer cells through MBOAT2

(A) *MBOAT2* mRNA expression in cancer patient samples (TCGA PanCancer Atlas Studies, cBioPortal). *MBOAT2* mRNA expression was batch normalized from Illumina HiSeq_RNASeqV2. Dashed line indicates median.

(B) Western blot analysis showing endogenous MBOAT2 expression in a panel of AR$^+$ and AR$^-$ PCa lines. AR$^+$ PCa lines were treated with DMSO or 5 μM ENZ for 48 h.

(C) Viability analysis of a panel of AR$^+$ and AR$^-$ PCa lines. Ferroptosis was induced by 3 μM RSL3 for 24 h.

(D) Visualization of AR and FOXA1 binding to the MBOAT2 ARE region (normalized by RPKM, GSE37345).

(E) ChIP-qPCR showing the occupancy of AR on the human *MBOAT2* ARE region in LnAR cells with indicated treatment for 24 h. DHT: 100 nM; ENZ: 5 μM.

(F) Western blot analysis showing MBOAT2 expression in LNCaP cells with indicated treatment for 48 h. DHT: 100 nM; ENZ: 5 μM.

(G) Western blot analysis showing MBOAT2 expression in LnAR-ishAR cells with or without Dox (1 μg/mL) treatment for 48 h.

(H) Western blot analysis showing MBOAT2 expression in PC3 and PC3-AR cells with or without DHT (100 nM) treatment for 48 h.

(I) Western blot analysis confirming MBOAT2 knockout in LnAR-gMBOAT2 cells.

(J) Viability analysis of LnAR-Cas9 and LnAR-gMBOAT2 cells with indicated RSL3 for 24 h.

(K and L) Quantification of differential PL-PUFAs (K) and PL-MUFAs (L) in LnAR-shNT and LnAR-ishMBOAT2 cells. See also Table S3.

Data are presented as mean ± SD, n = 3 biologically independent samples in (C), (E), and (J) or n = 5 biologically independent samples in (K) and (L). Statistical analysis was performed using two-way ANOVA in (C), one-way ANOVA in (E), or two-tailed t test in (K) and (L).

See also Figure S4.

AR antagonist sensitizes AR$^+$ prostate cancer to ferroptosis

Since upregulated MBOAT2 in AR$^+$ PCa promotes ferroptosis resistance, would AR antagonization sensitize the tumor cells to ferroptosis induction by downregulating MBOAT2, hence a potential therapeutic strategy? To test this possibility, we compared the ferroptosis sensitivity of LNCaP (representing castration-sensitive PCa) and LnAR (representing castration-resistant PCa [CRPC]) cells in normal medium and in medium with androgen depletion. Androgen deprivation diminished MBOAT2 expression and sensitized LNCaP cells to ferroptosis (Figures S5A and S5B). However, androgen deprivation did not significantly sensitize LnAR cells to ferroptosis (Figure S5C).

Although deprivation of androgen from culture medium did not sensitize CRPC LnAR cells to ferroptosis induction, we tested whether treatment with anti-AR agents can do so. ENZ is a second-generation, FDA-approved AR-targeted therapeutic agent that binds to the ligand-binding domain of AR, preventing AR nuclear translocation, thus suppressing the transcriptional activity of AR.[40] ARV-110 is a clinical stage PROTAC protein degrader selectively targeting AR.[41] Remarkably, both ENZ and ARV-110 inhibited endogenous MBOAT2 expression in a dose-dependent manner (Figures 5A, 5C, and S5H) and strongly sensitized multiple AR$^+$ PCa cell lines to RSL3-induced ferroptosis, including CRPC line LnAR (Figures 5A–5D and S5D–S5M). As expected, RSL3-induced lipid peroxidation was also potentiated by ENZ (Figure 5E).

Please cite this article in press as: Liang et al., Ferroptosis surveillance independent of GPX4 and differentially regulated by sex hormones, Cell (2023), https://doi.org/10.1016/j.cell.2023.05.003

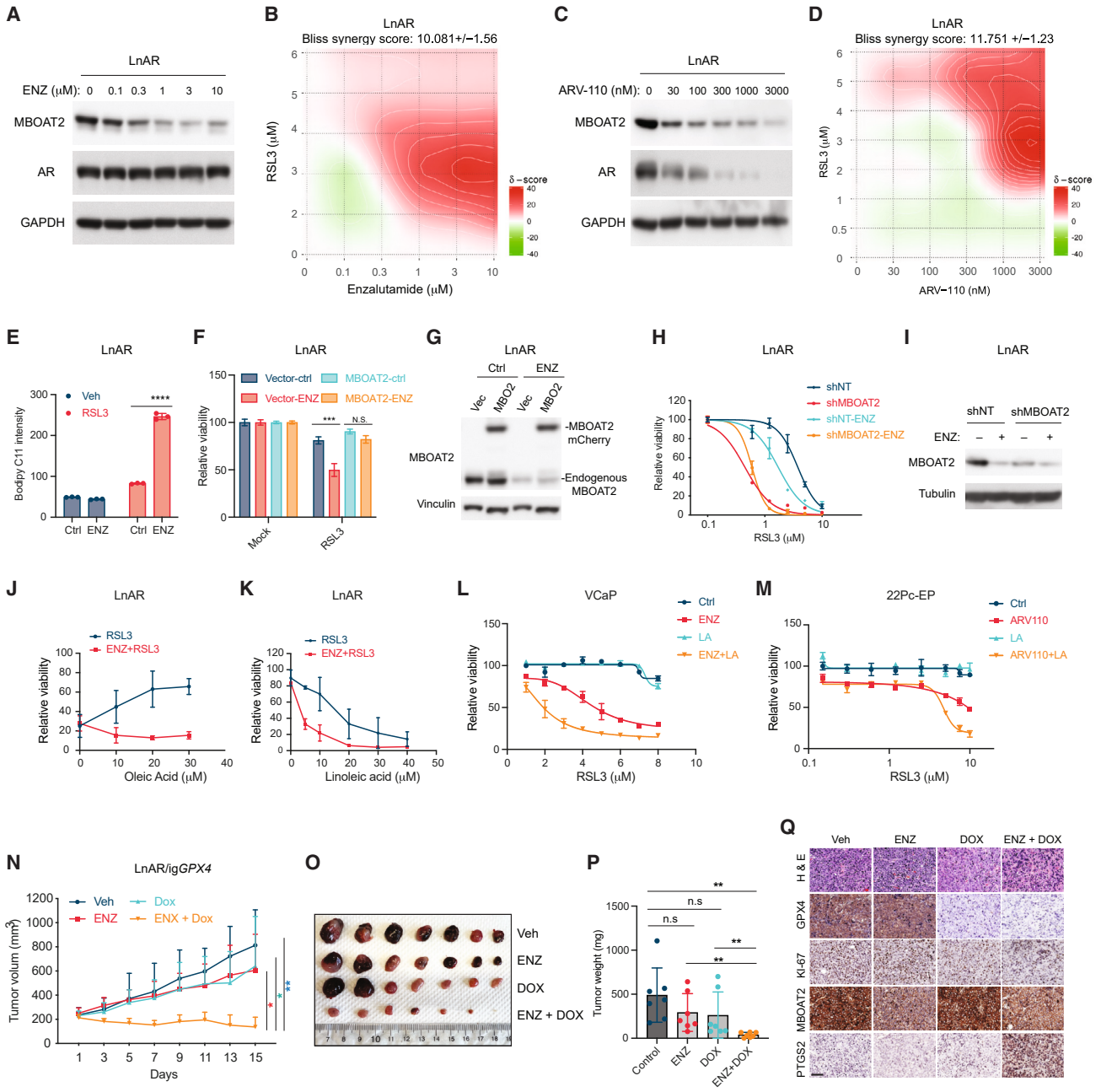

Figure 5. AR antagonist sensitizes AR$^+$ prostate cancer cells to ferroptosis

(A and C) Western blot showing MBOAT2 and AR expression in LnAR cells with indicated treatment for 48 h.

(B and D) Bliss synergy score surface plots of LnAR cells with indicated combination treatment. Cells were pretreated with indicated ENZ (B) or ARV-110 (D) for 48 h, followed by treatment with indicated concentration of RSL3 for 24 h. Synergy scores and plots were generated by SynergyFinder 3.0.

(E) Quantification of lipid peroxidation. LnAR cells were pretreated with DMSO control (Ctrl) or 5 μM ENZ for 48 h, followed by RSL3 (1 μM) for 3 h prior to labeling with BODIPY-C11.

(F) Viability analysis of LnAR cells harboring vector or MBOAT2 overexpression. Cells were pretreated with DMSO (Ctrl) or 5 μM ENZ for 48 h, followed by 1 μM RSL3 for 24 h.

(G) Western blot showing expression of endogenous and ectopic MBOAT2 in LnAR cells harboring either vector control or MBOAT2-mCherry. Cells were treated with 5 μM ENZ as indicated for 48 h.

(H) Viability of LnAR-shNT and LnAR-shMBOAT2 cells pretreated with DMSO or 5 μM ENZ for 48 h, followed by treatment with indicated concentration of RSL3 for 24 h.

(I) Western blot showing MBOAT2 expression in LnAR-shNT and LnAR-shMBOAT2 cells treated with 5 μM ENZ as indicated for 48 h.

(legend continued on next page)

Please cite this article in press as: Liang et al., Ferroptosis surveillance independent of GPX4 and differentially regulated by sex hormones, Cell (2023), https://doi.org/10.1016/j.cell.2023.05.003

To test whether ENZ can sensitize ferroptosis through suppressing MBOAT2 expression, we established LnAR cell line expressing ectopic MBOAT2 (transcription of ectopic MBOAT2 is not regulated by AR or ENZ) (Figure 5G). Indeed, ENZ only sensitized ferroptosis in control LnAR cells but not in LnAR cells expressing ectopic MBOAT2 (Figure 5F). Moreover, ENZ did not further sensitize ferroptosis in LnAR-shMBOAT2 cells (Figures 5H and 5I), confirming that ENZ sensitizes ferroptosis through downregulating endogenous MBOAT2.

We subsequently examined in AR^+ PCa cells whether ENZ could abolish the effect of exogenous MUFA on ferroptosis inhibition and promote the role of exogenous PUFA in potentiating ferroptosis. Indeed, although exogenous OA inhibited RSL3-induced ferroptosis in a dose-dependent manner in untreated LnAR cells, ENZ treatment abolished the protective function of OA (Figure 5J). Conversely, ENZ significantly enhanced ferroptosis in the presence of exogenous LA (Figures 5K–5M).

In the clinic, ENZ treatment will ultimately lead to ENZ resistance in patients through several possible mechanisms: (1) activation of AR-bypass signaling, in which other transcription factors (e.g., glucocorticoid receptor [GR]) are induced to substitute AR in order to activate a similar but distinguishable set of target genes[42,43]; (2) activation of AR-independent oncogenic signaling (reviewed in Watson et al.[44]); and (3) transition to a neuroendocrine prostate cancer (NEPC) phenotype.[44] An LnAR subline termed LREX′ acquired resistance to ENZ in a GR-dependent manner.[42] Interestingly, a subset of AR target genes are still responsive to AR signaling in LREX' cells, and we found that ENZ almost completely blocked MBOAT2 expression in these cells (Figure S5O). Importantly, although ENZ alone failed to decrease the viability of LREX' cells, it sensitized the cells to ferroptosis induction (Figures S5M and S5N), suggesting that the combination of ENZ with ferroptosis induction might overcome the resistance of AR^+ PCa to ENZ.

To test whether ENZ sensitizes CRPC to ferroptosis *in vivo*, hence a potential combination therapy, we established a LnAR-iCas9-gGPX4 (LnAR-igGPX4) cell line in which Cas9 expression can be induced by doxycycline (Dox). Similar to RSL3-induced ferroptosis, ferroptosis triggered by inducible GPX4 knockout in LnAR cells was also further potentiated by ENZ (Figures S5P and 5Q). We then generated an LnAR-igGPX4 xenograft model. Although Dox diet efficiently induced GPX4 knockout (Figure 5Q), and ENZ clearly decreased MBOAT2 expression in the tumors (Figure 5Q), Dox diet or ENZ alone only moderately inhibited tumor growth (Figures 5N–5P). In contrast, Dox diet in combination with ENZ completely inhibited tumor growth and caused notable tumor regression (Figures 5N–5P). As a marker of tumor ferroptosis, PTGS2 expression was significantly upregulated in the combination group (Figure 5Q).

MBOAT1 is an additional MUFA-preferred ferroptosis-suppressing LPLAT and is regulated by estrogen receptor (ER)

In HT1080-$GPX4^{KO}$ cells, SCD1 overexpression could promote cell survival even when MBOAT2 was knocked out (Figures S6A and S6B), suggesting the presence of other LPLAT(s) that can also catalyze PL-MUFA synthesis. There are 14 identified LPLATs with 10 from the 1-acylglycerol-3-phosphate O-acyltransferase (AGPAT) family and 4 from the MBOAT family.[45] We overexpressed 4 MBOAT family members (MBOAT1, 2, 5, and 7) and 1 AGPAT family member (LPCAT4), as well as DGAT1 (a MBOAT family member but not a LPLAT) as control, in HT1080 cells. In addition to MBOAT2, we found that MBOAT1, but not other tested enzymes, could also rescue cells from ferroptosis induced by GPX4 knockout or RSL3 (Figures 6A, 6B, and S6D). Moreover, MBOAT1 was able to support long-term culture of $GPX4^{KO}$ cells without trolox supplement (Figure S6C). Therefore, MBOAT1 is another LPLAT that can suppress ferroptosis independently of GPX4.

MBOAT1, also known as LPEAT1, preferentially transfers OA to lyso-PE and lyso-phosphatidylserine (PS).[27] We hypothesize that like MBOAT2, MBOAT1 suppresses ferroptosis through PL remodeling with a bias for PE-MUFAs. Indeed, ACC inhibitor TOFA or SCD1 inhibitor CAY10566 abolished the protection function of MBOAT1 overexpression (Figures 6C–6E), and the ferroptosis-suppressing activity of exogenous MUFAs was further potentiated by MBOAT1 overexpression (Figure S6E). In a targeted lipidomic analysis to measure relative abundance of several major PE-OAs and PE-AAs, we found that 3 out of 4 PE-OAs are significantly increased, while 3 out of 4 PE-AAs are significantly decreased (Figures 6F and 6G). Importantly, the increase of PE-OAs was very similar to the decrease of PE-AAs that share the same backbone of lyso-PE (e.g., PE P-16:0_18:1 vs. PE P-16:0_20:4; Figures 6H and 6I). Further, MBOAT1 significantly diminished RSL3-induced lipid peroxidation (Figure 6J), likely a consequence of PE-AA reduction.

Intriguingly and as opposed to MBOAT2, our database analysis indicates that MBOAT1 is highly expressed in female cancers, including ovarian cancer, BCa, and endometrial cancer (TCGA

(J and K) Viability analysis of LnAR cells pretreated with DMSO or 5 μM ENZ for 24 h, followed by incubation with indicated oleic acid (J) or linoleic acid (K) for 16 h. Subsequently, ferroptosis was induced by 10 μM RSL3 (J) or 2 μM RSL3 (K) for 24 h.

(L) Viability analysis of VCaP cells pretreated with DMSO or 5 μM ENZ for 24 h, followed by incubation with 10 μM LA for 16 h. Subsequently, ferroptosis was induced by indicated RSL3 for 24 h.

(M) Viability analysis of 22Pc-EP cells pretreated with DMSO or 1 μM ARV-110 for 24 h, followed by incubation with 10 μM LA for 16 h. Subsequently, ferroptosis was induced by indicated RSL3 for 24 h.

(N) Growth curves of xenograft tumors derived from LnAR-igGPX4 cells. Tumor-bearing mice were randomly divided into 4 groups: Veh (normal diet + vehicle), ENZ (normal diet + ENZ), DOX (Dox diet + vehicle), and ENZ + DOX (Dox diet + ENZ). See detail in STAR Methods. Mice were treated for 15 days.

(O and P) Images (O) and weight (P) of tumors with indicated treatment at day 15.

(Q) Representative H&E and immunostaining images of GPX4, Ki67, MBOAT2, and PTGS2 are shown from sections of xenograft tumors with indicated treatment. Scale bars, 100 μm.

Data are presented as mean ± SD, n = 3 biologically independent samples in (E), (F), (H), (J)–(L), and (M) or n = 7 biologically independent samples in (N) and (P). Statistical analysis was performed using one-way ANOVA in (F) and (P), two-way ANOVA in (N), and two-tailed t test in (E).

See also Figure S5.

Please cite this article in press as: Liang et al., Ferroptosis surveillance independent of GPX4 and differentially regulated by sex hormones, Cell (2023), https://doi.org/10.1016/j.cell.2023.05.003

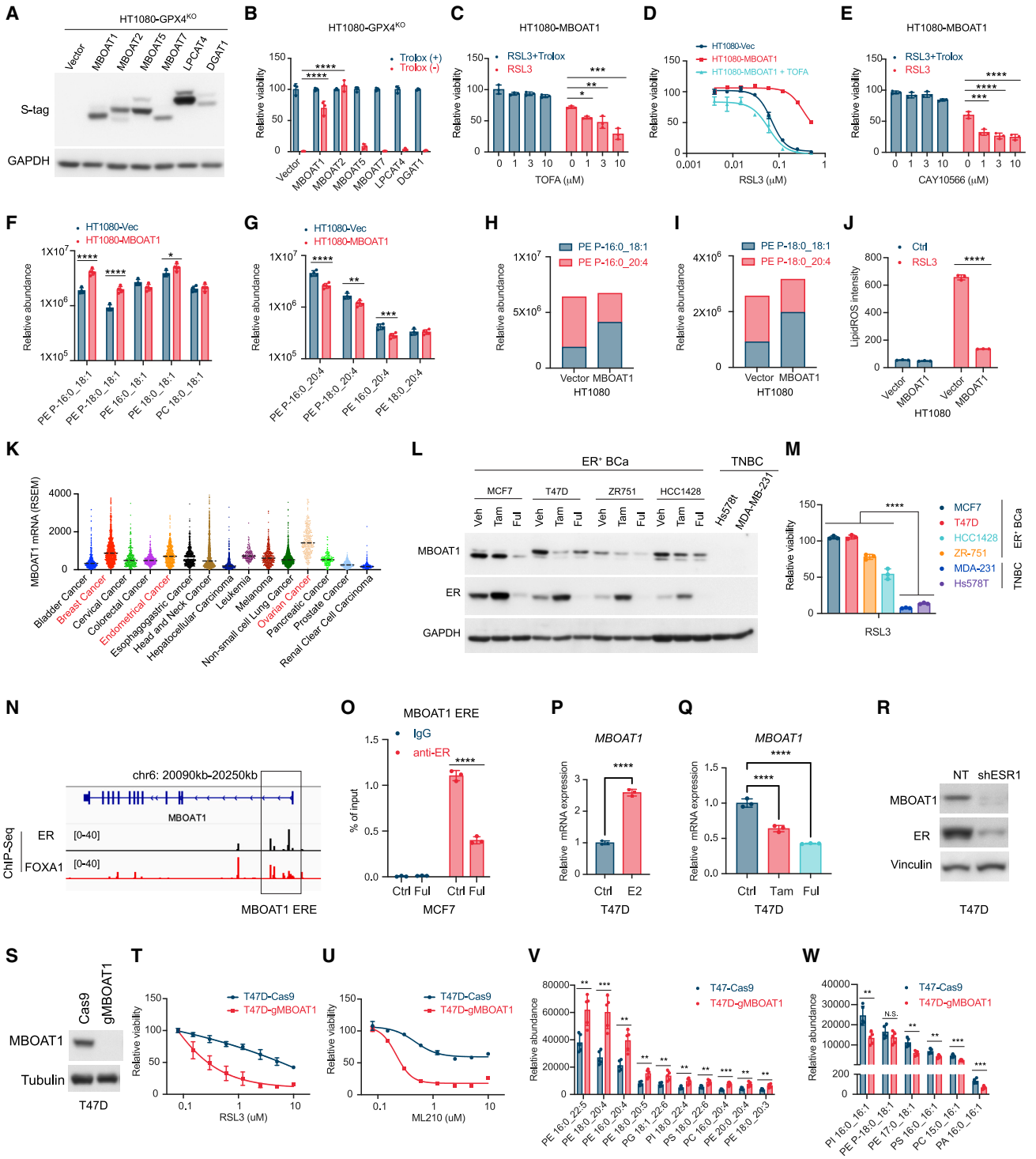

Figure 6. MBOAT1 suppresses ferroptosis and is regulated by ER signaling

(A) Western blot showing ectopic expression of indicated genes in HT1080-GPX4^{KO} cells.

(B) Viability analysis of HT1080-GPX4^{KO} cells ectopically overexpressing indicated genes. Cells were cultured in the presence of 100 μM trolox, and ferroptosis was induced by removing trolox for 24 h.

(C and E) Viability analysis of HT1080-MBOAT1 cells. Cells were pretreated with indicated concentrations of TOFA (C) or CAY10566 (E) for 24 h, followed by ferroptosis induction with 0.1 μM RSL3 for another 24 h in the presence or absence of trolox, as indicated.

(legend continued on next page)

Please cite this article in press as: Liang et al., Ferroptosis surveillance independent of GPX4 and differentially regulated by sex hormones, Cell (2023), https://doi.org/10.1016/j.cell.2023.05.003

PanCancer Atlas; Figure 6K), as well as in normal female tissues (e.g., fallopian tube, uterus, cervix, ovary, and mammary tissue; GTEx Portal; Figure S6F). This observation prompted us to examine whether MBOAT1 is regulated by ER signaling. In a panel of ER$^+$ BCa cell lines and triple-negative BCa (TNBC) cell lines, we found that MBOAT1 expression was uniquely upregulated in ER$^+$ BCa (Figure 6L) and correlated with the ferroptosis resistance state of ER$^+$ BCas (Figure 6M). Importantly, selective ER modulator (SERM) 4-hydroxyl-tamoxifen (Tam) and selective ER down-regulator (SERD) Ful decreased MBOAT1 expression in this panel of ER$^+$ BCas (Figure 6L). An analysis of ChIP-seq dataset (GSE72249)[46] revealed that ER and FOXA1 bind to a putative intronic estrogen response element (ERE) proximal to *MBOAT1* TSS (Figure 6N). Our ChIP-qPCR analysis confirmed binding of ER at *MBOAT1* ERE and further showed that Ful can decrease the binding of ER to this region (Figure 6O). Consistently, in ER$^+$ BCa T47D and MCF7 cells, estradiol (E2) upregulated *MBOAT1* mRNA, whereas Tam and Ful downregulated *MBOAT1* transcription (Figures 6P, 6Q, and S6G–S6J). Knockdown of ESR1 (encoding ER-alpha), or FOXA1, the functional partner of ER, also decreased MBOAT1 expression (Figures 6R, S6K, andS6L). Additionally, depletion of estrogen from culture medium inhibited MBOAT1 expression (Figures S6M and S6N). Taken together, MBOAT1 is a direct transcriptional target of ER. It should be emphasized that AR regulates MBOAT2 but not MBOAT1, whereas ER specifically regulates MBOAT1 but not MBOAT2 (see Figures S6O and S6P). These results suggest that MBOAT1 and MBOAT2 are differentially regulated to suppress ferroptosis in ER$^+$ and AR$^+$ tumors, respectively.

Consistent with the anti-ferroptotic role of MBOAT1, MBOAT1 elimination sensitized ER$^+$ BCa T47D cells and MCF7 cells to ferroptosis (Figures 6S–6U, S6Q, and S6R). Through lipidomic analysis, we found that MBOAT1 knockout altered PL profile in T47D cells with multiple PE-PUFAs significantly increased and various PL-MUFAs decreased (Table S4; Figures S6S, S6V, and S6W). Further, although exogenous LA failed to stimulate ferroptosis in parental T47D cells, it significantly promoted ferroptosis upon MBOAT1 knockout (Figure S6T).

Fulvestrant sensitizes hormone therapy-resistant ER$^+$ breast cancer to ferroptosis

Since ER upregulates MBOAT1 in ER$^+$ BCa and contributes to ferroptosis resistance, we wondered whether ER antagonization can sensitize ER$^+$ BCa to ferroptosis induction by downregulating MBOAT1. Indeed, ER degrader Ful significantly downregulated endogenous MBOAT1 expression, and sensitized tested ER$^+$ BCa cells to ferroptosis (Figures 7A–7F, S7A, and S7B). Remarkably, when LA was supplemented in culture medium, the effect of Ful on RSL3- or ML210-induced lipid peroxidation (Figure 7H) and ferroptosis (Figures 7G and S7A–S7E) was further enhanced. This sensitization effect of Ful was largely diminished by ectopic overexpression of MBOAT1 (Figures 7E, 7F, and S7C–S7E), indicating that Ful sensitizes ferroptosis through downregulating endogenous MBOAT1.

Some ER$^+$ BCa patients are resistant to ER-targeted therapies.[47] To study the underlying mechanism, ER$^+$ BCa cell lines resistant to ER-targeted therapies have been experimentally derived from ER$^+$ BCa cells initially sensitive to such therapies.[48] Interestingly, we found that a Ful-resistant MCF7 cell line (MCF7-FulR$^+$) and a Tam-resistant MCF7 cell line (MCF7-TamR$^+$) were still as responsive as parental MCF7 cells to Ful-mediated ER degradation and subsequent MBOAT1 downregulation (Figure 7I). This result prompted us to test whether the combination of ER inhibition with ferroptosis induction might be an effective therapy. As expected, estrogen depletion increased ferroptosis in MCF7-FulR$^+$ and MCF7-TamR$^+$ cells (Figure S7I). Notably, Ful but not Tam sensitized MCF7-FulR$^+$ and MCF7-TamR$^+$ cells to ferroptosis (Figure 7J). This might be because Tam and its analogs are RTAs, as reported previously.[49] Indeed, Tam inhibited ferroptosis in HT1080 cells induced by various FINs (Figures S7F–S7H). Similar to MCF7 cells, T47D-FulR$^+$ cells were also sensitized to ferroptosis upon Ful treatment

(D) Viability of HT1080-vector and HT1080-MBOAT1 cells with or without pretreatment of 5 μM TOFA for 24 h, followed by ferroptosis induction with indicated concentration of RSL3 for 24 h.
(F and G) Quantification of PE-MUFAs (F) and PE-PUFAs (G) in HT1080-Vec and HT1080-MBOAT1 cells.
(H and I) Stacked bars showing relative abundance of indicated PE-OAs and PE-AAs in HT1080-vector and HT1080-MBOAT1 cells.
(J) Quantification of lipid peroxidation. HT1080-vector or HT1080-MBOAT1 cells were treated with 0.1 μM RSL3 for 3 h prior to labeling with BODIPY-C11.
(K) *MBOAT1* mRNA expression of different cancer patient samples (TCGA PanCancer Atlas Studies, cBioportal). *MBOAT1* mRNA expression was batch normalized from Illumina HiSeq_RNASeqV2. Dashed line indicates median.
(L) Western blot showing endogenous MBOAT1 expression in a panel of ER$^+$ and triple-negative BCa lines. ER$^+$ BCa lines were either treated with DMSO, 5 μM Tam, or 0.5 μM Ful for 48 h.
(M) Viability analysis of a panel of ER$^+$ and triple-negative BCa lines. Ferroptosis was induced by 3 μM RSL3 for 24 h.
(N) Visualization of ER and FOXA1 binding to the MBOAT1 ERE region (normalized by RPKM, GSE72249).
(O) ChIP-qPCR showing the occupancy of ER on the human *MBOAT1* ERE region in MCF7 cells with indicated treatment for 24 h. Ful: 0.5 μM.
(P and Q) *MBOAT1* mRNA expression was detected by qRT-PCR in T47D cells treated with DMSO (Ctrl) or 100 nM E2 for 48 h (P); treated with DMSO control, 1 μM tamoxifen (Tam), or 0.5 μM fulvestrant (Ful) for 48 h (Q).
(R) Western blot showing MBOAT1 and ER expression in T47D-shNT and T47D-shESR1 cells.
(S) Western blot confirming MBOAT1 knockout in T47D-gMBOAT1 cells.
(T and U) Viability analysis of T47D-Cas9 and T47D-gMBOAT1 cells with indicated RSL3 (T) or ML210 (U) for 24 h.
(V and W) Quantification of differential PL-PUFAs (V) and PL-MUFAs (W) in T47D-Cas9 and T47D-gMBOAT1 cells. See also Table S4.
Data are presented as mean ± SD, n = 3 biological independent replicates in (B)–(G), (J), (M), (O)–(Q), (T), and (U) or n = 5 biological independent replicates in (V) and (W). Statistical analysis was performed using one-way ANOVA in (B), (C), (E), and (Q), two-tailed t test in (F), (G), (J), (O), (P), (V), and (W), and two-way ANOVA in (M).
See also Figure S6.

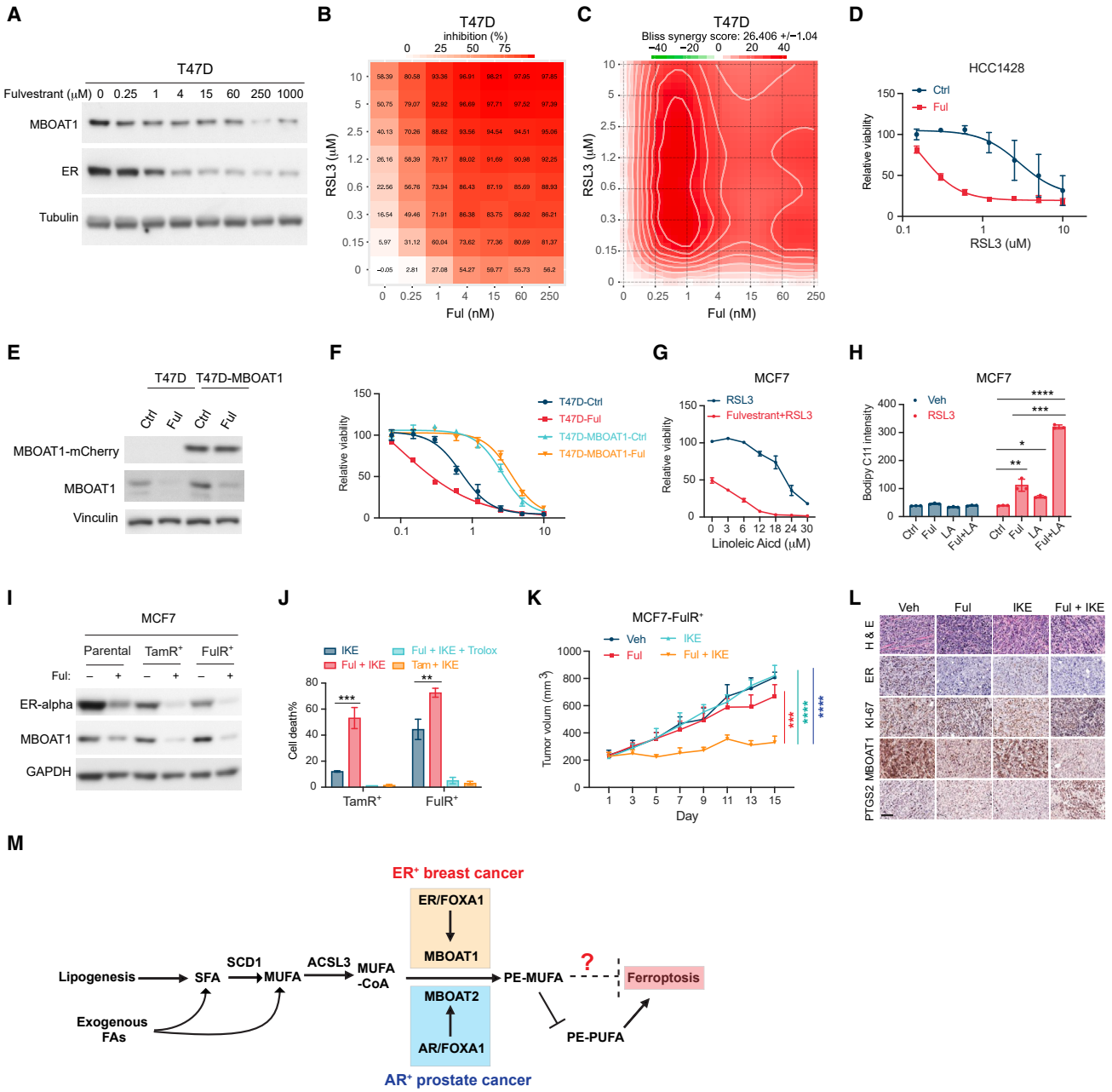

Figure 7. Fulvestrant sensitizes hormone therapy-resistant ER+ breast cancer to ferroptosis

(A) Western blot showing MBOAT1 and ER expression in T47D cells with indicated treatment for 48 h.

(B and C) Dose-response matrix (B) and Bliss synergy score surface plots (C) of T47D cells with a combination of Ful and RSL3 treatment. Cells were pretreated with indicated Ful for 48 h, followed by treatment with indicated concentration of RSL3 for 24 h. Matrix, synergy scores, and plots were generated by SynergyFinder 3.0.

(D) Viability of HCC1428 cells pretreated with or without 0.5 μM Ful for 48 h, followed by ferroptosis induction with indicated RSL3 for 24 h.

(E) Western blot showing expression of endogenous and ectopic MBOAT1 in T47D cells harboring either vector control or MBOAT1-mCherry. Cells were treated with 0.5μM Ful as indicated for 48 h.

(F) Viability analysis of T47D cells harboring vector or MBOAT1 overexpression. Cells were pretreated with DMSO (Ctrl) or Ful for 48 h, followed by ferroptosis induction with indicated RSL3 for 24 h.

(G) Viability of MCF7 cells pretreated with or without 0.5 μM Ful for 24 h, followed by incubation with indicated concentration LA for 24 h. Subsequently, ferroptosis was induced by 1 μM RSL3 for 24 h.

(H) Quantification of lipid peroxidation in MCF7 cells pretreated with Ful for 24 h, followed by incubation with indicated concentration LA for 24 h. Subsequently, ferroptosis was induced by 1 μM RSL3 for 4 h prior to labeling with BODIPY-C11.

(legend continued on next page)

Please cite this article in press as: Liang et al., Ferroptosis surveillance independent of GPX4 and differentially regulated by sex hormones, Cell (2023), https://doi.org/10.1016/j.cell.2023.05.003

(Figure S7J). Thus, we focused on Ful instead of Tam in subsequent experiments.

To test the potential therapeutical effect of Ful in combination with FIN IKE on Ful-resistant ER$^+$ BCa, we established a MCF7-FulR$^+$ xenograft model. Ful or IKE alone did not inhibit tumor growth (Figure 7K). In contrast, a combination of Ful and IKE significantly inhibited the tumor growth (Figure 7K) without affecting normal animal weight (Figure S7K). Consistently, while Ful alone led to MBOAT1 downregulation in tumor tissues, only the combination of Ful with IKE caused an upregulation of PTGS2 expression (Figure 7L). Therefore, a combination of ER targeting with ferroptosis induction represents a potential therapy for the treatment of ER$^+$ BCa resistant to ER-targeted monotherapies.

DISCUSSION

Multiple surveillance mechanisms have evolved to suppress cellular PL peroxidation and subsequent ferroptosis, making these mechanisms pivotal points for ferroptosis regulation.[1,2] GPX4 and various RTA-generating enzymes mediate two well-characterized surveillance mechanisms. In this study, we discovered another ferroptosis surveillance mechanism mediated by MBOAT1/2-catalyzed cellular PL remodeling (Figure 7M). Intriguingly, although MBOAT1 and MBOAT2 appear to inhibit ferroptosis via the same biochemical route, they are differentially regulated by sex hormone signaling, suggesting distinctive biological function.

Conceptually, this finding is important for the field of ferroptosis, as it reveals a surveillance mechanism independent of GPX4 and RTAs. GPX4-mediated and RTA-mediated surveillances act at specific stages of PL peroxidation by reducing PL peroxides and terminating the PL oxidation loop, respectively. Different from these two mechanisms, MBOAT1/2 function upstream by altering cellular PL profile, causing an increase of PL-MUFAs and a corresponding decrease of PL-PUFAs, the substrate of PL peroxidation. However, is decreasing the substrate of PL peroxidation the sole mechanism underlying MBOAT1/2-mediated suppression of ferroptosis? This is debatable, because MBOAT1/2 overexpression could lead to highly potent ferroptosis inhibition and sustained cell survival even upon GPX4/FSP1 double knockout, but it only caused a relatively modest decrease of PL-PUFAs (Figures 3D and 6G). Therefore, does ferroptosis require a high level of PL-PUFAs, but only at certain specific membrane "microdomains," hence the change of PL-PUFA versus PL-MUFA at the whole-cell level remains to be modest? Alternatively, a fundamentally distinctive possibility is that PL-MUFAs inhibit ferroptosis via mechanism(s) beyond simply replacing PL-PUFAs in the cellular lipidome, such as via regulating a yet-to-be identified mediator. All these questions warrant further investigation.

Biologically, differential regulation of MBOAT1 and MBOAT2 by ER signaling and AR signaling, respectively, provides intriguing insights into the potential role of ferroptosis suppression in specific contexts related to sex hormone signaling. Based on these observations, an interesting hypothesis is that in biological processes highly regulated by these sex hormones, such as reproductive development, MBOAT1/2 need to be upregulated to suppress ferroptosis in relevant organs. This hypothesis is testable experimentally. Further, as the biochemical activity of MBOAT1 and MBOAT2 in both PL anabolism and ferroptosis suppression is likely to be quite similar, it is intriguing that the organism uses these two different genes to mediate hormone signaling of opposite sex, instead of putting the same gene under regulation by both classes of sex hormones. Therefore, it is possible that in addition to their differential regulation by sex hormone signaling, these two enzymes may exert certain distinctive and sex-specific biochemical functions.

These findings are highly relevant to cancer. Ferroptosis induction has emerged as a promising cancer therapeutic approach. To induce ferroptosis, one can inhibit the ferroptosis surveillance pathways, especially if cancer cells upregulate such mechanisms and develop addiction to them. Therefore, our discovery that MBOAT1/2 are upregulated in specific cancers suggests that they are potential therapeutic targets. Inhibition of MBOAT1/2 will promote ferroptosis more effectively than inhibition of SCD1, a potential therapeutic target under active investigation.[50] Targeting of SCD1 is at least partially effective, because SCD1 suppresses ferroptosis by generating MUFAs endogenously.[16,51,52] However, cancer cells might also acquire MUFAs extracellularly if they reside in a MUFA-rich environment—under such condition, targeting SCD1 might not have any therapeutic efficacy. On the other hand, both endogenous and exogenous MUFAs require downstream MBOAT1/2 activity to inhibit ferroptosis, suggesting they are more effective therapeutic targets. Further, although it is not known whether MBOAT1/2 are involved in the onset or progression of sex hormone-driven cancers, we demonstrated that sex hormone-induced MBOAT1/2 upregulation renders these tumors more resistant to ferroptosis, and conversely, antagonizing ER/AR signaling sensitizes these cancer cells to ferroptosis induction. Remarkably, even in ER$^+$/AR$^+$ cancer cells resistant to ER/AR

(I) Western blot of MBOAT1 and ER-alpha in MCF7-parental, MCF7-TamR$^+$, and MCF7-FulR$^+$ cells with or without 0.5 μM Ful treatment for 48 h.
(J) Cell death analysis of MCF7-TamR$^+$ and MCF7-FulR$^+$ cells that were pretreated with either DMSO, or 1 μM Ful, or 10 μM Tam for 48 h, and followed with either 10 μM IKE or 10 μM IKE plus 100 μM trolox for 24 h.
(K) Growth curves of tumors derived from MCF7-FulR$^+$ cells in xenograft mouse models. Tumors were grown to around 250 mm^3, at which point mice were randomly divided into 4 groups: vehicle, Ful (5 mg, s.c. injection), IKE (40 mg/kg i.p. injection), and Ful + IKE. Mice were treated for 15 days.
(L) Representative H&E and immunostaining images of ER, Ki67, MBOAT1, and PTGS2 are shown from sections of tumors derived from MCF7-FulR$^+$ cells with indicated treatment. Scale bars, 100 μm.
(M) Working model showing ER signaling upregulates MBOAT1 expression in ER$^+$ cancer cells, while AR signaling upregulates MBOAT2 expression in AR$^+$ cancer cells. MBOAT1/2 can utilize endogenous or exogenous MUFA to suppress ferroptosis through phospholipid remodeling.
Data are presented as mean ± SD, n = 3 biologically independent samples in (D), (F)–(H), and (J) or n = 5–6 biologically independent samples in (K). Statistical analysis was performed using one-way ANOVA in (H), two-way ANOVA in (K), and two-tailed t test in (J).
See also Figure S7.

inhibitors, if the regulation of MBOAT1/2 by sex hormones persists, this combination therapy might still be effective in inducing tumor ferroptosis. This is clinically relevant, as there are ER^+ BCa patients and AR^+ prostate cancer patients who are not responsive to corresponding hormonal therapies.[53,54]

Limitations of the study

There are 14 genes encoding putative LPLAT enzymes. Although the current study has demonstrated that MBOAT1/2 can function as ferroptosis suppressors, we have not exhaustedly tested all LPLATs for their potential role in ferroptosis and their regulation by cancer signaling. In fact, biochemical and cellular properties of most of these enzymes, including their substrate selectivity and tissue distribution, have not be fully defined, limiting further investigation of the role of these LPLATs in ferroptosis under biologically relevant contexts.

The current study has provided insights into two potential combination cancer therapies. However, until now, ferroptosis-inducing agents for clinical use have not been developed, thus limiting the investigation at the preclinical stage.

STAR★METHODS

Detailed methods are provided in the online version of this paper and include the following:

- KEY RESOURCES TABLE
- RESOURCE AVAILABILITY
  - Lead contact
  - Materials availability
  - Data and code availability
- EXPERIMENTAL MODEL AND SUBJECT DETAILS
  - Mice
  - Cell lines
  - Constructs
- METHOD DETAILS
  - Production of lentiviral and retroviral infectious particles
  - Generation of CRISPR knockout cells
  - Generation of shRNA expression cells
  - Generation of stable expression cells
  - CRISPR activation screen and data analysis
  - 3′-RNA Quant-seq and data analysis
- LIPIDOMIC ANALYSES
  - Sample preparation
  - LC conditions
  - MS conditions
  - Data preprocessing and statistical analysis
  - Structural assignment of identified lipids
  - Chromatin immunoprecipitation (ChIP)
  - Generating of drug resistant breast cancer cells
  - Cell death assay
  - Cell viability assay
  - Measurement of Lipid Peroxidation
  - Western Blot
  - qRT-PCR
  - Animal Models
  - Immunohistochemistry
- QUANTIFICATION AND STATISTICAL ANALYSIS

SUPPLEMENTAL INFORMATION

Supplemental information can be found online at https://doi.org/10.1016/j.cell.2023.05.003.

ACKNOWLEDGMENTS

We thank MSKCC Integrated Genomics Operation (IGO) core for deep sequencing, MSKCC Bioinformatic core for data analysis, MSKCC Pathology Core for assistance with IHC, and MSKCC Antitumor Assessment core for assistance with xenograft experiments. We also thank Drs. Jason Lewis, Marilyn Resh, and Nancy Du for providing crucial cell lines and plasmids. We thank members of the Jiang lab for critical reading and suggestions. This work is supported by NIH R01CA204232, NIH R01CA258622, and NIH R01CA166413 (to X.J.); NIH R35CA253059 (to W.G.); NIH R35CA209896 (to B.R.S); and NCI cancer center core grant P30 CA008748 to MSKCC. Z.Z. is an HHMI Fellow of the Damon Runyon Cancer Research Foundation, supported by DRG-2467-22.

AUTHOR CONTRIBUTIONS

Conceptualization, D.L. and X.J.; experiment, D.L, Y.F., F.Z., H.W., Z.Z, J.K., and Y.C.; funding acquisition, X.J.; data analysis, D.L., F.Z., H.W., W.G., B.R.S., and X.J.; writing, D.L. and X.J.

DECLARATION OF INTERESTS

D.L. is an inventor on a patent related to autophagy. B.R.S. is an inventor on patents and patent applications involving small-molecule drug discovery and ferroptosis; has co-founded and serves as a consultant to Inzen Therapeutics, Exarta Therapeutics, and ProJenX, Inc.; serves as a consultant to Weatherwax Biotechnologies Corporation and Akin Gump Strauss Hauer & Feld LLP; and receives sponsored research support from Sumitomo Dainippon Pharma Oncology. X.J. is an inventor on patents related to autophagy and cell death and holds equity of and consults for Exarta Therapeutics and Lime Therapeutics.

Received: November 28, 2022
Revised: March 20, 2023
Accepted: May 4, 2023
Published: June 1, 2023

REFERENCES

1. Stockwell, B.R. (2022). Ferroptosis turns 10: Emerging mechanisms, physiological functions, and therapeutic applications. Cell *185*, 2401–2421. https://doi.org/10.1016/j.cell.2022.06.003.
2. Jiang, X., Stockwell, B.R., and Conrad, M. (2021). Ferroptosis: mechanisms, biology and role in disease. Nat. Rev. Mol. Cell Biol. *22*, 266–282. https://doi.org/10.1038/s41580-020-00324-8.
3. Green, D.R. (2019). The coming decade of cell death research: five riddles. Cell *177*, 1094–1107. https://doi.org/10.1016/j.cell.2019.04.024.
4. Yang, W.S., SriRamaratnam, R., Welsch, M.E., Shimada, K., Skouta, R., Viswanathan, V.S., Cheah, J.H., Clemons, P.A., Shamji, A.F., Clish, C.B., et al. (2014). Regulation of ferroptotic cancer cell death by GPX4. Cell *156*, 317–331. https://doi.org/10.1016/j.cell.2013.12.010.
5. Dixon, S.J., Lemberg, K.M., Lamprecht, M.R., Skouta, R., Zaitsev, E.M., Gleason, C.E., Patel, D.N., Bauer, A.J., Cantley, A.M., Yang, W.S., et al. (2012). Ferroptosis: an iron-dependent form of nonapoptotic cell death. Cell *149*, 1060–1072. https://doi.org/10.1016/j.cell.2012.03.042.
6. Bersuker, K., Hendricks, J.M., Li, Z., Magtanong, L., Ford, B., Tang, P.H., Roberts, M.A., Tong, B., Maimone, T.J., Zoncu, R., et al. (2019). The CoQ oxidoreductase FSP1 acts parallel to GPX4 to inhibit ferroptosis. Nature *575*, 688–692. https://doi.org/10.1038/s41586-019-1705-2.

7. Doll, S., Freitas, F.P., Shah, R., Aldrovandi, M., da Silva, M.C., Ingold, I., Goya Grocin, A., Xavier da Silva, T.N., Panzilius, E., Scheel, C.H., et al. (2019). FSP1 is a glutathione-independent ferroptosis suppressor. Nature *575*, 693–698. https://doi.org/10.1038/s41586-019-1707-0.

8. Mao, C., Liu, X., Zhang, Y., Lei, G., Yan, Y., Lee, H., Koppula, P., Wu, S., Zhuang, L., Fang, B., et al. (2021). DHODH-mediated ferroptosis defence is a targetable vulnerability in cancer. Nature *593*, 586–590. https://doi.org/10.1038/s41586-021-03539-7.

9. Soula, M., Weber, R.A., Zilka, O., Alwaseem, H., La, K., Yen, F., Molina, H., Garcia-Bermudez, J., Pratt, D.A., and Birsoy, K. (2020). Metabolic determinants of cancer cell sensitivity to canonical ferroptosis inducers. Nat. Chem. Biol. *16*, 1351–1360. https://doi.org/10.1038/s41589-020-0613-y.

10. Kraft, V.A.N., Bezjian, C.T., Pfeiffer, S., Ringelstetter, L., Müller, C., Zandkarimi, F., Merl-Pham, J., Bao, X., Anastasov, N., Kössl, J., et al. (2020). GTP cyclohydrolase 1/tetrahydrobiopterin counteract ferroptosis through lipid remodeling. ACS Cent. Sci. *6*, 41–53. https://doi.org/10.1021/acscentsci.9b01063.

11. Kapralov, A.A., Yang, Q., Dar, H.H., Tyurina, Y.Y., Anthonymuthu, T.S., Kim, R., St Croix, C.M., Mikulska-Ruminska, K., Liu, B., Shrivastava, I.H., et al. (2020). Redox lipid reprogramming commands susceptibility of macrophages and microglia to ferroptotic death. Nat. Chem. Biol. *16*, 278–290. https://doi.org/10.1038/s41589-019-0462-8.

12. Jiang, L., Kon, N., Li, T., Wang, S.J., Su, T., Hibshoosh, H., Baer, R., and Gu, W. (2015). Ferroptosis as a p53-mediated activity during tumour suppression. Nature *520*, 57–62. https://doi.org/10.1038/nature14344.

13. Zhang, Y., Shi, J., Liu, X., Feng, L., Gong, Z., Koppula, P., Sirohi, K., Li, X., Wei, Y., Lee, H., et al. (2018). BAP1 links metabolic regulation of ferroptosis to tumour suppression. Nat. Cell Biol. *20*, 1181–1192. https://doi.org/10.1038/s41556-018-0178-0.

14. Gao, M., Yi, J., Zhu, J., Minikes, A.M., Monian, P., Thompson, C.B., and Jiang, X. (2019). Role of mitochondria in ferroptosis. Mol. Cell *73*. 354–363.e3. https://doi.org/10.1016/j.molcel.2018.10.042.

15. Wu, J., Minikes, A.M., Gao, M., Bian, H., Li, Y., Stockwell, B.R., Chen, Z.N., and Jiang, X. (2019). Intercellular interaction dictates cancer cell ferroptosis via NF2-YAP signalling. Nature *572*, 402–406. https://doi.org/10.1038/s41586-019-1426-6.

16. Yi, J., Zhu, J., Wu, J., Thompson, C.B., and Jiang, X. (2020). Oncogenic activation of PI3K-AKT-mTOR signaling suppresses ferroptosis via SREBP-mediated lipogenesis. Proc. Natl. Acad. Sci. USA *117*, 31189–31197. https://doi.org/10.1073/pnas.2017152117.

17. Wang, W., Green, M., Choi, J.E., Gijón, M., Kennedy, P.D., Johnson, J.K., Liao, P., Lang, X., Kryczek, I., Sell, A., et al. (2019). CD8(+) T cells regulate tumour ferroptosis during cancer immunotherapy. Nature *569*, 270–274. https://doi.org/10.1038/s41586-019-1170-y.

18. Badgley, M.A., Kremer, D.M., Maurer, H.C., DelGiorno, K.E., Lee, H.J., Purohit, V., Sagalovskiy, I.R., Ma, A., Kapilian, J., Firl, C.E.M., et al. (2020). Cysteine depletion induces pancreatic tumor ferroptosis in mice. Science *368*, 85–89. https://doi.org/10.1126/science.aaw9872.

19. Zhang, Y., Tan, H., Daniels, J.D., Zandkarimi, F., Liu, H., Brown, L.M., Uchida, K., O'Connor, O.A., and Stockwell, B.R. (2019). Imidazole ketone erastin induces ferroptosis and slows tumor growth in a mouse lymphoma model. Cell Chem. Biol. *26*. 623–633.e9. https://doi.org/10.1016/j.chembiol.2019.01.008.

20. Arensman, M.D., Yang, X.S., Leahy, D.M., Toral-Barza, L., Mileski, M., Rosfjord, E.C., Wang, F., Deng, S., Myers, J.S., Abraham, R.T., et al. (2019). Cystine-glutamate antiporter xCT deficiency suppresses tumor growth while preserving antitumor immunity. Proc. Natl. Acad. Sci. USA *116*, 9533–9542. https://doi.org/10.1073/pnas.1814932116.

21. Wiernicki, B., Maschalidi, S., Pinney, J., Adjemian, S., Vanden Berghe, T., Ravichandran, K.S., and Vandenabeele, P. (2022). Cancer cells dying from ferroptosis impede dendritic cell-mediated anti-tumor immunity. Nat. Commun. *13*, 3676. https://doi.org/10.1038/s41467-022-31218-2.

22. Kim, R., Hashimoto, A., Markosyan, N., Tyurin, V.A., Tyurina, Y.Y., Kar, G., Fu, S., Sehgal, M., Garcia-Gerique, L., Kossenkov, A., et al. (2022). Ferroptosis of tumour neutrophils causes immune suppression in cancer. Nature *612*, 338–346. https://doi.org/10.1038/s41586-022-05443-0.

23. Liao, P., Wang, W., Wang, W., Kryczek, I., Li, X., Bian, Y., Sell, A., Wei, S., Grove, S., Johnson, J.K., et al. (2022). CD8(+) T cells and fatty acids orchestrate tumor ferroptosis and immunity via ACSL4. Cancer Cell *40*. 365–378.e6. https://doi.org/10.1016/j.ccell.2022.02.003.

24. Doll, S., Proneth, B., Tyurina, Y.Y., Panzilius, E., Kobayashi, S., Ingold, I., Irmler, M., Beckers, J., Aichler, M., Walch, A., et al. (2017). ACSL4 dictates ferroptosis sensitivity by shaping cellular lipid composition. Nat. Chem. Biol. *13*, 91–98. https://doi.org/10.1038/nchembio.2239.

25. Kagan, V.E., Mao, G., Qu, F., Angeli, J.P., Doll, S., Croix, C.S., Dar, H.H., Liu, B., Tyurin, V.A., Ritov, V.B., et al. (2017). Oxidized arachidonic and adrenic PEs navigate cells to ferroptosis. Nat. Chem. Biol. *13*, 81–90. https://doi.org/10.1038/nchembio.2238.

26. Gijón, M.A., Riekhof, W.R., Zarini, S., Murphy, R.C., and Voelker, D.R. (2008). Lysophospholipid acyltransferases and arachidonate recycling in human neutrophils. J. Biol. Chem. *283*, 30235–30245. https://doi.org/10.1074/jbc.M806194200.

27. Hishikawa, D., Shindou, H., Kobayashi, S., Nakanishi, H., Taguchi, R., and Shimizu, T. (2008). Discovery of a lysophospholipid acyltransferase family essential for membrane asymmetry and diversity. Proc. Natl. Acad. Sci. USA *105*, 2830–2835. https://doi.org/10.1073/pnas.0712245105.

28. Valentin, E., Singer, A.G., Ghomashchi, F., Lazdunski, M., Gelb, M.H., and Lambeau, G. (2000). Cloning and recombinant expression of human group IIF-secreted phospholipase A(2). Biochem. Biophys. Res. Commun. *279*, 223–228. https://doi.org/10.1006/bbrc.2000.3908.

29. O'Donnell, V.B. (2022). New appreciation for an old pathway: the Lands Cycle moves into new arenas in health and disease. Biochem. Soc. Trans. *50*, 1–11. https://doi.org/10.1042/BST20210579.

30. Liang, D., Minikes, A.M., and Jiang, X. (2022). Ferroptosis at the intersection of lipid metabolism and cellular signaling. Mol. Cell *82*, 2215–2227. https://doi.org/10.1016/j.molcel.2022.03.022.

31. Dixon, S.J., Winter, G.E., Musavi, L.S., Lee, E.D., Snijder, B., Rebsamen, M., Superti-Furga, G., and Stockwell, B.R. (2015). Human haploid cell genetics reveals roles for lipid metabolism genes in nonapoptotic cell death. ACS Chem. Biol. *10*, 1604–1609. https://doi.org/10.1021/acschembio.5b00245.

32. Beharier, O., Tyurin, V.A., Goff, J.P., Guerrero-Santoro, J., Kajiwara, K., Chu, T., Tyurina, Y.Y., St Croix, C.M., Wallace, C.T., Parry, S., et al. (2020). PLA2G6 guards placental trophoblasts against ferroptotic injury. Proc. Natl. Acad. Sci. USA *117*, 27319–27328. https://doi.org/10.1073/pnas.2009201117.

33. Chen, D., Chu, B., Yang, X., Liu, Z., Jin, Y., Kon, N., Rabadan, R., Jiang, X., Stockwell, B.R., and Gu, W. (2021). iPLA2beta-mediated lipid detoxification controls p53-driven ferroptosis independent of GPX4. Nat. Commun. *12*, 3644. https://doi.org/10.1038/s41467-021-23902-6.

34. Sun, W.Y., Tyurin, V.A., Mikulska-Ruminska, K., Shrivastava, I.H., Anthonymuthu, T.S., Zhai, Y.J., Pan, M.H., Gong, H.B., Lu, D.H., Sun, J., et al. (2021). Phospholipase iPLA2beta averts ferroptosis by eliminating a redox lipid death signal. Nat. Chem. Biol. *17*, 465–476. https://doi.org/10.1038/s41589-020-00734-x.

35. Magtanong, L., Ko, P.J., To, M., Cao, J.Y., Forcina, G.C., Tarangelo, A., Ward, C.C., Cho, K., Patti, G.J., Nomura, D.K., et al. (2019). Exogenous monounsaturated fatty acids promote a ferroptosis-resistant cell state. Cell Chem. Biol. *26*. 420–432.e9. https://doi.org/10.1016/j.chembiol.2018.11.016.

36. Guijas, C., Astudillo, A.M., Gil-de-Gómez, L., Rubio, J.M., Balboa, M.A., and Balsinde, J. (2012). Phospholipid sources for adrenic acid mobilization in RAW 264.7 macrophages. Comparison with arachidonic acid. Biochim. Biophys. Acta *1821*, 1386–1393. https://doi.org/10.1016/j.bbalip.2012.07.010.

37. Ma, X., Xiao, L., Liu, L., Ye, L., Su, P., Bi, E., Wang, Q., Yang, M., Qian, J., and Yi, Q. (2021). CD36-mediated ferroptosis dampens intratumoral CD8(+) T cell effector function and impairs their antitumor ability. Cell Metab. *33*. 1001–1012.e5. https://doi.org/10.1016/j.cmet.2021.02.015.

38. Jin, H.J., Zhao, J.C., Wu, L., Kim, J., and Yu, J. (2014). Cooperativity and equilibrium with FOXA1 define the androgen receptor transcriptional program. Nat. Commun. *5*, 3972. https://doi.org/10.1038/ncomms4972.

39. Karthaus, W.R., Hofree, M., Choi, D., Linton, E.L., Turkekul, M., Bejnood, A., Carver, B., Gopalan, A., Abida, W., Laudone, V., et al. (2020). Regenerative potential of prostate luminal cells revealed by single-cell analysis. Science *368*, 497–505. https://doi.org/10.1126/science.aay0267.

40. Tran, C., Ouk, S., Clegg, N.J., Chen, Y., Watson, P.A., Arora, V., Wongvipat, J., Smith-Jones, P.M., Yoo, D., Kwon, A., et al. (2009). Development of a second-generation antiandrogen for treatment of advanced prostate cancer. Science *324*, 787–790. https://doi.org/10.1126/science.1168175.

41. Mullard, A. (2019). First targeted protein degrader hits the clinic. Nat. Rev. Drug Discov. https://doi.org/10.1038/d41573-019-00043-6.

42. Arora, V.K., Schenkein, E., Murali, R., Subudhi, S.K., Wongvipat, J., Balbas, M.D., Shah, N., Cai, L., Efstathiou, E., Logothetis, C., et al. (2013). Glucocorticoid receptor confers resistance to antiandrogens by bypassing androgen receptor blockade. Cell *155*, 1309–1322. https://doi.org/10.1016/j.cell.2013.11.012.

43. Shah, N., Wang, P., Wongvipat, J., Karthaus, W.R., Abida, W., Armenia, J., Rockowitz, S., Drier, Y., Bernstein, B.E., Long, H.W., et al. (2017). Regulation of the glucocorticoid receptor via a BET-dependent enhancer drives antiandrogen resistance in prostate cancer. eLife *6*. https://doi.org/10.7554/eLife.27861.

44. Watson, P.A., Arora, V.K., and Sawyers, C.L. (2015). Emerging mechanisms of resistance to androgen receptor inhibitors in prostate cancer. Nat. Rev. Cancer *15*, 701–711. https://doi.org/10.1038/nrc4016.

45. Valentine, W.J., Yanagida, K., Kawana, H., Kono, N., Noda, N.N., Aoki, J., and Shindou, H. (2022). Update and nomenclature proposal for mammalian lysophospholipid acyltransferases, which create membrane phospholipid diversity. J. Biol. Chem. *298*, 101470. https://doi.org/10.1016/j.jbc.2021.101470.

46. Swinstead, E.E., Miranda, T.B., Paakinaho, V., Baek, S., Goldstein, I., Hawkins, M., Karpova, T.S., Ball, D., Mazza, D., Lavis, L.D., et al. (2016). Steroid receptors reprogram FoxA1 occupancy through dynamic chromatin transitions. Cell *165*, 593–605. https://doi.org/10.1016/j.cell.2016.02.067.

47. Dittmer, J. (2021). Nuclear mechanisms involved in endocrine resistance. Front. Oncol. *11*, 736597. https://doi.org/10.3389/fonc.2021.736597.

48. Cheng, G.J., Leung, E.Y., and Singleton, D.C. (2022). In vitro breast cancer models for studying mechanisms of resistance to endocrine therapy. Explor. Target Antitumor Ther. *3*, 297–320. https://doi.org/10.37349/etat.2022.00084.

49. Dubey, R.K., Tyurina, Y.Y., Tyurin, V.A., Gillespie, D.G., Branch, R.A., Jackson, E.K., and Kagan, V.E. (1999). Estrogen and tamoxifen metabolites protect smooth muscle cell membrane phospholipids against peroxidation and inhibit cell growth. Circ. Res. *84*, 229–239. https://doi.org/10.1161/01.res.84.2.229.

50. Tracz-Gaszewska, Z., and Dobrzyn, P. (2019). Stearoyl-CoA desaturase 1 as a therapeutic target for the treatment of cancer. Cancers (Basel) *11*. https://doi.org/10.3390/cancers11070948.

51. Tesfay, L., Paul, B.T., Konstorum, A., Deng, Z., Cox, A.O., Lee, J., Furdui, C.M., Hegde, P., Torti, F.M., and Torti, S.V. (2019). Stearoyl-CoA desaturase 1 protects ovarian cancer cells from ferroptotic cell death. Cancer Res. *79*, 5355–5366. https://doi.org/10.1158/0008-5472.CAN-19-0369.

52. Wohlhieter, C.A., Richards, A.L., Uddin, F., Hulton, C.H., Quintanal-Villalonga, À., Martin, A., de Stanchina, E., Bhanot, U., Asher, M., Shah, N.S., et al. (2020). Concurrent mutations in STK11 and KEAP1 promote ferroptosis protection and SCD1 dependence in lung cancer. Cell Rep. *33*, 108444. https://doi.org/10.1016/j.celrep.2020.108444.

53. Hanker, A.B., Sudhan, D.R., and Arteaga, C.L. (2020). Overcoming endocrine resistance in breast cancer. Cancer Cell *37*, 496–513. https://doi.org/10.1016/j.ccell.2020.03.009.

54. Schmidt, K.T., Huitema, A.D.R., Chau, C.H., and Figg, W.D. (2021). Resistance to second-generation androgen receptor antagonists in prostate cancer. Nat. Rev. Urol. *18*, 209–226. https://doi.org/10.1038/s41585-021-00438-4.

55. Konermann, S., Brigham, M.D., Trevino, A.E., Joung, J., Abudayyeh, O.O., Barcena, C., Hsu, P.D., Habib, N., Gootenberg, J.S., Nishimasu, H., et al. (2015). Genome-scale transcriptional activation by an engineered CRISPR-Cas9 complex. Nature *517*, 583–588. https://doi.org/10.1038/nature14136.

56. Sanson, K.R., Hanna, R.E., Hegde, M., Donovan, K.F., Strand, C., Sullender, M.E., Vaimberg, E.W., Goodale, A., Root, D.E., Piccioni, F., et al. (2018). Optimized libraries for CRISPR-Cas9 genetic screens with multiple modalities. Nat. Commun. *9*, 5416. https://doi.org/10.1038/s41467-018-07901-8.

57. Henry, K.E., Dacek, M.M., Dilling, T.R., Caen, J.D., Fox, I.L., Evans, M.J., and Lewis, J.S. (2019). A PET imaging strategy for interrogating target engagement and oncogene status in pancreatic cancer. Clin. Cancer Res. *25*, 166–176. https://doi.org/10.1158/1078-0432.CCR-18-1485.

58. Zhang, Z., Karthaus, W.R., Lee, Y.S., Gao, V.R., Wu, C., Russo, J.W., Liu, M., Mota, J.M., Abida, W., Linton, E., et al. (2020). Tumor microenvironment-derived NRG1 promotes antiandrogen resistance in prostate cancer. Cancer Cell *38*. 279–296.e9. https://doi.org/10.1016/j.ccell.2020.06.005.

59. Li, W., Xu, H., Xiao, T., Cong, L., Love, M.I., Zhang, F., Irizarry, R.A., Liu, J.S., Brown, M., and Liu, X.S. (2014). MAGeCK enables robust identification of essential genes from genome-scale CRISPR/Cas9 knockout screens. Genome Biol. *15*, 554. https://doi.org/10.1186/s13059-014-0554-4.

60. Wickham, H. (2016). ggplot2: Elegant Graphics for Data Analysis (Springer-Verlag New York).

61. Ianevski, A., Giri, A.K., and Aittokallio, T. (2022). SynergyFinder 3.0: an interactive analysis and consensus interpretation of multi-drug synergies across multiple samples. Nucleic Acids Res. *50*, W739–W743. https://doi.org/10.1093/nar/gkac382.

62. Chen, Y., Chi, P., Rockowitz, S., Iaquinta, P.J., Shamu, T., Shukla, S., Gao, D., Sirota, I., Carver, B.S., Wongvipat, J., et al. (2013). ETS factors reprogram the androgen receptor cistrome and prime prostate tumorigenesis in response to PTEN loss. Nat. Med. *19*, 1023–1029. https://doi.org/10.1038/nm.3216.

63. Karthaus, W.R., Iaquinta, P.J., Drost, J., Gracanin, A., van Boxtel, R., Wongvipat, J., Dowling, C.M., Gao, D., Begthel, H., Sachs, N., et al. (2014). Identification of multipotent luminal progenitor cells in human prostate organoid cultures. Cell *159*, 163–175. https://doi.org/10.1016/j.cell.2014.08.017.

64. Fellmann, C., Hoffmann, T., Sridhar, V., Hopfgartner, B., Muhar, M., Roth, M., Lai, D.Y., Barbosa, I.A., Kwon, J.S., Guan, Y., et al. (2013). An optimized microRNA backbone for effective single-copy RNAi. Cell Rep. *5*, 1704–1713. https://doi.org/10.1016/j.celrep.2013.11.020.

65. Kim, D., Langmead, B., and Salzberg, S.L. (2015). HISAT: a fast spliced aligner with low memory requirements. Nat. Methods *12*, 357–360. https://doi.org/10.1038/nmeth.3317.

66. Liao, Y., Smyth, G.K., and Shi, W. (2014). featureCounts: an efficient general purpose program for assigning sequence reads to genomic features. Bioinformatics *30*, 923–930. https://doi.org/10.1093/bioinformatics/btt656.

67. Love, M.I., Huber, W., and Anders, S. (2014). Moderated estimation of fold change and dispersion for RNA-seq data with DESeq2. Genome Biol. *15*, 550. https://doi.org/10.1186/s13059-014-0550-8.

68. Chong, J., Soufan, O., Li, C., Caraus, I., Li, S., Bourque, G., Wishart, D.S., and Xia, J. (2018). MetaboAnalyst 4.0: towards more transparent and

integrative metabolomics analysis. Nucleic Acids Res. *46*, W486–W494. https://doi.org/10.1093/nar/gky310.

69. Fahy, E., Subramaniam, S., Murphy, R.C., Nishijima, M., Raetz, C.R., Shimizu, T., Spener, F., van Meer, G., Wakelam, M.J., and Dennis, E.A. (2009). Update of the LIPID MAPS comprehensive classification system for lipids. J. Lipid Res. *50* (*Suppl*), S9–S14. https://doi.org/10.1194/jlr.R800095-JLR200.

70. Wang, H., Fan, Z., Shliaha, P.V., Miele, M., Hendrickson, R.C., Jiang, X., and Helin, K. (2023). H3K4me3 regulates RNA polymerase II promoter-proximal pause-release. Nature *615*, 339–348. https://doi.org/10.1038/s41586-023-05780-8.

Please cite this article in press as: Liang et al., Ferroptosis surveillance independent of GPX4 and differentially regulated by sex hormones, Cell (2023), https://doi.org/10.1016/j.cell.2023.05.003

STAR★METHODS

KEY RESOURCES TABLE

REAGENT or RESOURCE	SOURCE	IDENTIFIER
Antibodies		
Anti-MBOAT2	Novus Biologicals	Cat # NBP182236; RRID:AB_11033200
Anti-MBOAT1	Fisher Scientific	Cat # PIPA5-43193; RRID:AB_2607164
Anti-GPX4	Abcam	Cat # ab125066; RRID:AB_10973901
Anti-SCD1	Abcam	Cat # Ab39969; RRID:AB_945374
Anti-Androgen Receptor	Cell Signaling	Cat #5153; RRID:AB_10691711
Anti-Estrogen Receptor	Cell Signaling	Cat #13258; RRID:AB_2632959
Anti-FSP1	Santa Cruz	Cat # sc-377120; RRID:AB_2893240
Anti-Flag	Sigma-Aldrich	Cat # F1804; RRID:AB_262044
Anti-Vinculin	Sigma-Aldrich	Cat # V9131; RRID:AB_477629
Anti-GAPDH	Cell Signaling	Cat # 2118; RRID:AB_561053
Anti-Cox-2 (PTGS2)	Abcam	Cat #Ab16701; RRID:AB_443436
Anti-FOXA1	Cell Signaling	Cat #53528; RRID:AB_2799438
Anti-NOS2	Biolegend	Cat #690902; RRID:AB_2629826
Anti-Ki67	Cell Signaling	Cat #9027; RRID:AB_2636984
Bacterial and virus strains		
Lenti dCAS-VP64_Blast	Konermann et al.[55]	Addgene viral prep (# 61425-LV)
Human Calabrese CRISPR activation pooled library set A	Sanson et al.[56]	Addgene #92379-LVC
DH5alpha	Fisher Scientific	Cat # 18265017
E. coli Stbl3	Fisher Scientific	Cat# C737303
Chemicals, peptides, and recombinant proteins		
Liproxstatin-1	Cayman Chemical	Cat #17730-50
17β-Estradiol	Cayman Chemical	Cat #10006315-500
Fulvestrant	Cayman Chemical	Cat #10011269-5
ML-210	Cayman Chemical	Cat #23282-5
Imidazole Ketone Erastin	Cayman Chemical	Cat #27088-5
(1S,3R)-RSL3	Cayman Chemical	Cat #19288-10
Imidazole ketone erastin,98%	MedChem Express	Cat # HY-114481
Enzalutamide	MedChem Express	Cat # HY-70002
TOFA	Santa Cruz	Cat # sc-200653
CAY 10566	Santa Cruz	Cat # sc-205109
Erastin	Selleck Chemicals	Cat # S7242-5mg
Dihydrotestosterone (DHT)	Selleck Chemicals	Cat # S4757-10mM
Enzalutamide (MDV3100)	Selleck Chemicals	Cat # S1250-5mg
Ferrostatin-1	Sigma	Cat # SML0583-5MG
Oleic Acid-Albumin from bovine serum	Sigma-Aldrich	Cat # O3008-5ML
Linoleic Acid-Albumin from bovine serum albumin	Sigma-Aldrich	Cat # L9530-5ML
Doxycycline Hyclate, Suitable for Cell Culture	Sigma-Aldrich	Cat # D5207-5G
Butylated hydroxytoluene, ≥99%, FCC, FG	Sigma-Aldrich	Cat # W218405-1KG-K
Fulvestrant Inj 50 mg/mL (250 mg), 5 mL syringe	SKI Drug - Main Pharmacy	Cat #74711367
BODIPY® 581/591 C11 (Lipid Peroxidation Sensor)	Molecular Probe	Cat # D3861
SYTOX™ Green Nucleic Acid Stain	Fisher Scientific	Cat # S7020

(*Continued on next page*)

Please cite this article in press as: Liang et al., Ferroptosis surveillance independent of GPX4 and differentially regulated by sex hormones, Cell (2023), https://doi.org/10.1016/j.cell.2023.05.003

Continued

REAGENT or RESOURCE	SOURCE	IDENTIFIER
Fetal Bovine Serum, charcoal stripped	Fisher Scientific	Cat # A3382101
Tetracycline Negative Fetal Bovine Serum	Gemini Bio-Products	Cat # 100-800
Puromycin	Sigma-Aldrich	Cat # 540222
Blasticidin	InvivoGen	Cat # ant-bl-1
SuperSignal™ West Femto Maximum Sensitivity Substrate	Thermo Fisher Scientific	Cat # 34094
Clarity Western ECL Substrate	Bio-Rad	Cat # 1705061
Lipofectamine™ 3000 Transfection Reagent	Thermo Fisher Scientific	Cat # L3000008
IQ™ SYBR® Green Supermix	Bio-Rad	Cat # 1708882
Trizol™ Reagent	Fisher Scientific	Cat # 15596026
TaKaRa Ex Taq® DNA Polymerase (250 units)	Takara	Cat # RR001A
Agencourt AMPure XP, 5 mL	Beckman Coulter	Cat # A63880
T4 DNA Ligase	NEB	Cat # M0202M
Phusion High Fidelity DNA Polymerase	Fisher Scientific	Cat # F530L
Splash® Lipidomics® Mass Spec Standard	Avanti Ploar Lipids, INC.	Cat#330707
Isopropanol, Optima LC-MS grade	Fisher Scientific	Cat#A461-1
Water, Optima LC-MS grade	Fisher Scientific	Cat#W6212
Acetonitrile, Optima LC-MS grade	Fisher Scientific	Cat#A955
Ammonium acetate, Optima LC-MS grade	Fisher Scientific	Cat#A11450
Acetic acid, Optima LC-MS grade	Fisher Scientific	Cat#A11350
ERCC RNA Spike-In Mix 1	Fisher Scientific	Cat# 4456740
Critical commercial assays		
Iscript™ cDNA Synthesis Kit	Bio-Rad	Cat # 1708891
PureYield™ Plasmid Miniprep System	Promega	Cat # A1222
PureLink™ HiPure Plasmid Midiprep Kit	Invitrogen	Cat # K210005
CellTiter-Glo® Luminescent Cell Viability Assay	Promega	Cat # G7572
QIAamp DNA Blood Midi Kit	Qiagen	Cat # 51183
Iq™ SYBR	Bio-Rad	Cat # 1708882
QuantSeq 3′-mRNA Seq Library Prep Kit FWD for Illumina	Lexogen	SKU: 015.96
Retrievagen A antigen retrieval system	BD Biosciences	Cat# 550524
Experimental models: Cell lines		
Human: Lenti-X™ 293T Cell Line	Clonetech	Cat# 632180
Human: HT1080	ATCC	N/A
Human: HT1080-GPX4^{KO}	Gao et al.[14]	N/A
Human: HT1080-GPX4/FSP1^{DKO}	This paper	N/A
Human: SUIT-2	Henry et al.[57]	N/A
Human: HPAC	ATCC (provided by Nancy Du)	N/A
Human: AsPC-1	ATCC (provided by Merilyn Resh)	N/A
Human: BxPC-3	ATCC	N/A
Human: MIA PaCa2	ATCC	N/A
Human: PANC-1	ATCC	N/A
Human: Panc 05.04	ATCC (provided by Merilyn Resh)	N/A
Human: Hs766T	ATCC (provided by Merilyn Resh)	N/A
Human: Capan-1	ATCC (provided by Jason Lewis)	N/A
Human: LNCaP	Charles Sawyers	N/A
Human: LNCaP/AR (LnAR)	Charles Sawyers	N/A

(*Continued on next page*)

Please cite this article in press as: Liang et al., Ferroptosis surveillance independent of GPX4 and differentially regulated by sex hormones, Cell (2023), https://doi.org/10.1016/j.cell.2023.05.003

Continued

REAGENT or RESOURCE	SOURCE	IDENTIFIER
Human: LREX'	Charles Sawyers Arora et al.[42]	N/A
Human: 22Pc-EP	Charles Sawyers Zhang et al.[58]	N/A
Human: PC3	ATCC	N/A
Human: VCaP	ATCC	N/A
Human: DU145	ATCC	N/A
Human: MCF7	ATCC	N/A
Human: MCF7-Cas9 (parental)	This paper	N/A
Human: MCF7-Cas9 (Fulvestrant resistant)	This paper	N/A
Human: MCF7-Cas9 (Tamoxifen resistant)	This paper	N/A
Human: T47D	ATCC	N/A
Human: T47D (Fulvestrant resistant)	This paper	N/A
Human: HCC1428	ATCC (provided by Merilyn Resh)	N/A
Human: ZR-751	ATCC	N/A
Mouse: normal prostate organoid 819	Charles Sawyers	N/A
Experimental models: Organisms/strains		
5-6 weeks old male athymic nu/nu mice	Charles River Laboratories	N/A
5-6 weeks old female NOD/SCID mice	ENVIGO	N/A
Oligonucleotides		
Human-MBOAT1-qPCR-F: GGTTTCCACAGCTTGCCAGAAC	IDT	N/A
Human-MBOAT1-qPCR-R: GGTTTCCACAGCTTGCCAGAAC	IDT	N/A
Human-MBOAT2-qPCR-F: CTCGCTGGGACTTAATTTCCAA	IDT	N/A
Human-MBOAT2-qPCR-R: GGTTCGTTCATAACACACCCTT	IDT	N/A
Human-GAPDH-qPCR-F: ACAACTTTGGTATCGTGGAAGG	IDT	N/A
Human-GAPDH-qPCR-R: GCCATCACGCCACAGTTTC	IDT	N/A
Guide-F: TTGTGGAAAGGACGAAACACCG	IDT	N/A
Guide-R: TCTACTATTCTTTCCCCTGCACTGT	IDT	N/A
Mouse-Ar-qPCR-F: CCTTGGATGGAGAACTACTCCG	IDT	N/A
Mouse-Ar-qPCR-R: TCCGTAGTGACAGCCAGAAGCT	IDT	N/A
Mouse-Nkx3.1-qPCR-F: CGCGGAGACACCGACTGAACC	IDT	N/A
Mouse-Nkx3.1-qPCR-R: TTCTGTGGCTGCTTGGTGACCT	IDT	N/A
Mouse-Fkbp5-qPCR-F: GATTGCCGAGATGTGGTGTTCG	IDT	N/A
Mouse-Fkbp5-qPCR-R: GGCTTCTCCAAAACCATAGCGTG	IDT	N/A
Mouse-Tmprss2-qPCR-F: AAGTCCTCAGGAGCACTGTGCA	IDT	N/A
Mouse-Tmprss2-qPCR-R: CAGAACCTCCAAAGCAAGACAGC	IDT	N/A
Mouse-Mboat2-qPCR-F: CTCCGTCGCAGAGGGGATTA	IDT	N/A
Mouse-Mboat2-qPCR-R: GCAATGTAGTCTTTGTAGGAGCA	IDT	N/A
Mouse-Gapdh-qPCR-F: TGGCCTTCCGTGTTCCTAC	IDT	N/A
Mouse-Gapdh-qPCR-R: GAGTTGCTGTTGAAGTCGCA	IDT	N/A
MBOAT2-ChIP-F1: GTAGGTTTGGACTGGCAGCA	IDT	N/A
MBOAT2-ChIP-R1: CGTAGCACCACGCATTACTC	IDT	N/A
MBOAT1-ChIP-F1: CTCCAGCAGGAGTGAGTGTG	IDT	N/A
MBOAT1-ChIP-R1: CTTCCAAACTCGCAAGCCAC	IDT	N/A
Recombinant DNA		
Plasmid: gag/pol	Addgene	Cat# 14887
Plasmid: pCMV-VSV-G	Addgene	Cat# 8454

(*Continued on next page*)

Please cite this article in press as: Liang et al., Ferroptosis surveillance independent of GPX4 and differentially regulated by sex hormones, Cell (2023), https://doi.org/10.1016/j.cell.2023.05.003

Continued

REAGENT or RESOURCE	SOURCE	IDENTIFIER
Plasmid: pCMV-dR8.2 dvpr	Addgene	Cat# 8455
Plasmid: lentiCas9-Blast	Addgene	Cat# 52962
Plasmid: GCH1_pLX307	Addgene	Cat# 98336
Plasmid: pLIX403-hNOS2	Addgene	Cat# 110800
Plasmid: AAVS1 T2 CRIPR in pX330	Addgene	Cat# 72833
Plasmid: pAAVS1-tet-iCas9-BFP2	Addgene	Cat# 125519
Plasmid: ACSL3 cDNA ORF Clone	GenScript	OHu17295
Plasmid: MBOAT1 cDNA ORF Clone	GenScript	OHu00733
Plasmid: MBOAT2 cDNA ORF Clone	GenScript	OHu06224
Plasmid: MBOAT5 cDNA ORF Clone	GenScript	OHu05005
Plasmid: MBOAT7 cDNA ORF Clone	GenScript	OHu21224
Plasmid: FSP1 cDNA ORF Clone	GenScript	OHu10901
Plasmid: PLA2G2F cDNA ORF Clone	GenScript	OHu17317D
Plasmid: LPCAT4 cDNA ORF Clone	GenScript	OHu07050
Plasmid: pTURN-SCD1	Yi et al.[16]	N/A
Plasmid: pQCIP-SCD1	This paper	N/A
Plasmid: pQCIP-ACSL3	This paper	N/A
Plasmid: pQCIP-MBOAT1	This paper	N/A
Plasmid: pQCIP-MBOAT1-mCherry	This paper	N/A
Plasmid: pQCIP-MBOAT2	This paper	N/A
Plasmid: pQCIP-MBOAT2-mCherry	This paper	N/A
Plasmid: pQCIP-MBOAT5-mCherry	This paper	N/A
Plasmid: pQCIP-MBOAT7-mCherry	This paper	N/A
Plasmid: PQCIP-DGAT1-mCherry	This paper	N/A
Plasmid: pQCIP-FSP1	This paper	N/A
Plasmid: pWZL_AR-Blast	This paper	N/A
Plasmid LT3G-ishMBO2 (GCTCTTACAAAGACTACATTA)	This paper	N/A
Plasmid LT3G-ishAR (GCCAGCAGAAATGATTGCA)	This paper	N/A
Plasmid: shMBOAT2#1 (GCTCTTACAAAGACTACATTA)	MSKCC gene editing core	TRCN0000035240
Plasmid: shMBOAT2#2 (TTTACAGCTCCTGGTATTATT)	MSKCC gene editing core	TRCN0000370550
Plasmid: shACSL3#1 (GTGATGAAAGAATTACCGAAT)	MSKCC gene editing core	TRCN0000045530
Plasmid: shACSL3#2 (TGCTCTTTGTGGTTGGATCTA)	MSKCC gene editing core	TRCN0000045532
Plasmid: shMBOAT1#1 (CCTCAGACTCTGAACTCTATT)	MSKCC gene editing core	TRCN0000035315
Plasmid: shESR1 (GTGTGCCTCAAATCTATTATT)	MSKCC gene editing core	TRCN0000338158
Plasmid: pLKO_FOXA1_#1	Addgene	Cat# 70095
Plasmid: pLKO_FOXA1_#2	Addgene	Cat# 70096
Plasmid: sgSCD1#1 (GAGACGATGCCCCTCTACTTGG)	Sigma	HS5000004019
Plasmid: sgSCD1#2 (TACTATTTTGTCAGTGCCCTGG)	Sigma	HS5000004020
Plasmid: sgMBOAT2#1 (CTTTGTACAAGAAAGTGTAAGG)	Sigma	HS5000029185
Plasmid: sgMBOAT2#2 (TACTGCTTTGTGTTTGCTCTGG)	Sigma	HS5000029186
Plasmid: sgMBOAT1#1 (TCTGTGCATCTTTTTGTGCTGG)	Sigma	HS5000018673
Plasmid: sgMBOAT1#2 (TCTGAGTGACAATCATCAGAGG)	Sigma	HS5000018674
Plasmid: sgGPX4-Blast (CACGCCCGATACGCTGAGTG)	Gao et al.[14]	N/A
Plasmid: sgGPX4-Puro (TGATCTCTTCGTTACTCCCTGG)	Sigma	HS5000001523
Plasmid: sgAIFM2 (TAAGAAATGAATGTCTTTTTGG)	Sigma	HS5000029901
Software and algorithms		
Illustrator 2022	Adobe	N/A
Prism 9.0	GraphPad	N/A
Trim Galore (v0.5.0)	Babraham Institute	RRID:SCR_011847

(*Continued on next page*)

Please cite this article in press as: Liang et al., Ferroptosis surveillance independent of GPX4 and differentially regulated by sex hormones, Cell (2023), https://doi.org/10.1016/j.cell.2023.05.003

Continued

REAGENT or RESOURCE	SOURCE	IDENTIFIER
Picard (v 2.19.0)	Broad Institute	RRID:SCR_006525
RSEM	Dewey lab	RRID:SCR_013027
STAR (v 2.7.5a)	Alexander Dobin	RRID:SCR_004463
clusterProfiler (v3.18.1)	Guangchuang Yu	RRID:SCR_016884
R (v 4.0.5)	R project	RRID:SCR_001905
FlowJo v10	FlowJo, LLC	RRID:SCR_008520
Progenesis QI	Waters-Nonlinear Dynamics	https://www.nonlinear.com/progenesis/qi/
MassLynx, version 4.2	Waters	https://www.waters.com/waters/en_US/MassLynx-MS-Software/nav.htm?locale=en_US&cid=513662
MetaboAnalyst, 5.0	MetaboAnalyst software	https://www.metaboanalyst.ca/MetaboAnalyst/ModuleView.xhtml
MAGeCK (version 0.5.9)	Li et al.[59]	N/A
ggplot2	Wickham[60]	https://ggplot2.tidyverse.org
Synergyfinder 3.0	Ianvevsk et al.[61]	https://synergyfinder.fimm.fi/
Deposited Data		
Lipidomic data	This paper	Mendeley Data (https://doi.org/10.17632/n9y2vtpxkt.1)
ChIP-Seq data	Jin et al.[38] Swinstead et al.[46]	GSE37345 GSE72249
Single Cell RNA seq Data	Karthaus et al.[39]	GSE146811 DUOS-000115

RESOURCE AVAILABILITY

Lead contact

Further information and requests for resources and reagents should be directed to and will be fulfilled by the lead contact, Xuejun Jiang (jiangx@mskcc.org)

Materials availability

Plasmids generated in this study are available from the lead contact upon request.

Data and code availability

- Lipidomics data, western blot data, and drug combination treatment data have been deposited at Mendely Data (https://doi.org/10.17632/n9y2vtpxkt.1).
- This paper analyses existing, publicly available ChIP-Seq and single cell RNA-seq data. The accession numbers for these datasets are listed in the key resources table.
- This paper does not report original code.
- Any additional information required to reanalyze the data reported in this paper is available from the lead contact upon request.

EXPERIMENTAL MODEL AND SUBJECT DETAILS

Mice

5-6 weeks old male athymic nu/nu mice (Charles River Laboratories) were used for prostate cancer xenograft model. 5-6 weeks old female NOD/SCID mice (ENVIGO) were used for breast cancer xenograft model. Memorial Sloan Kettering Cancer Center Institutional Animal Care and Use Committee approved all procedures in accordance with the Guide for the Care and Use of Animals. All mice were housed in pathogen-free facilities, in a 12-hour light/dark cycle in ventilated cages, with chow and water supply ad libitum.

Please cite this article in press as: Liang et al., Ferroptosis surveillance independent of GPX4 and differentially regulated by sex hormones, Cell (2023), https://doi.org/10.1016/j.cell.2023.05.003

Cell lines

HT1080, 293T, HPAC, MIA PaCa-2, PANC-1, Hs766T, Panc 05.04, Capan-1, 22Pc-EP, VCaP, MCF7, PC3, DU145 cells, and their derived cell lines were cultured in DMEM (provided by Media Preparation Core Facility of MSKCC) with 10% Fetal bovine serum (Gibco), 2 mM L-glutamine and 100 u/mL Penicillin/Streptomycin (Gibco) at 37 °C and 5% CO_2. HT1080-GPX4^{KO} cells and their derived cell lines were maintained with 100μM Trolox in the medium.

SUIT-2, BxPC3, AsPC-1, LNCaP, LnAR, LREX', T47D, ZR751, HCC1428 cells, and their derived cell lines were cultured in RPMI (provided by Media Preparation Core Facility of MSKCC) with 10% Fetal bovine serum (Gibco), 2 mM L-glutamine and 100 u/mL Penicillin/Streptomycin (Gibco) at 37 °C and 5% CO_2. LnAR-igGPX4 cells were cultured in RPMI with 10% Tetracycline negative FBS (Gemini Bio-Products).

Normal mouse prostate organoid 819 was derived from the littermate control of PTEN-Flox/Flox, LSL-ERG mice from a mixed background.[62] 819 organoids were maintained according to established organoid culture protocol.[63]

All commercially obtained cells were authenticated by the vendors or by other groups who published these cells. All cell lines used in this study were regularly checked for the presence of mycoplasma by PCR.

Constructs

MBOAT2, PLA2G2F, FSP1, ACSL3, MBOAT1, MBOAT5, MBOAT7, LPCAT3 cDNAs (GenScript, with Flag-tag at C-terminus), or SCD1, DGAT1 cDNAs were subcloned into the pQCXIP, pQCXIB, or pQCXIP-mCherry (mCherry is fused with inserted gene at C-terminus). AR cDNA was subcloned into pWZL Blast myc plasmid (Addgene #10674).

Site directed mutagenesis of MBOAT2 (H373A) was performed and verified by sanger sequencing. LT3G-ishMBOAT2 (target sequence: GCTCTTACAAAGACTACATTA) and LT3G-ishAR (target sequence: GCCAGCAGAAATGATTGCA) were made by inserting miR-E shMBOAT2 or miR-E shAR fragment into LT3GEPIR vector (Addgene # 111177) as reported.[64]

METHOD DETAILS

Production of lentiviral and retroviral infectious particles

Retroviruses were produced by co-transfecting retroviral plasmid, packaging plasmid (gag/pol, Addgene#14887), and pCMV-VSV-G (Addgene #8454) plasmid into 293T cells by Lipofectamine 3000 reagents. Lentiviruses were produced by co-transfecting lentiviral plasmid, packaging plasmid (pCMV-dR8.2 dvpr, Addgene#8455), and pCMV-VSV-G (Addgene #8454) plasmid into 293T cells by lipofectamine 3000 reagents. The supernatants containing infectious particles were collected 48 h post transfection and passed through 0.45-μm filter.

Generation of CRISPR knockout cells

HT1080-GPX4^{KO} cells were previously established by our lab through transient transfection of sgGPX4 and spCas9 in HT1080 cells.[14] HT1080-GPX4^{KO}-Cas9 cells were generated by infecting HT1080-GPX4^{KO} cells with lentiCas9-Blast (Addgene #52962) lentivirus and selecting with 20μg/ml Blasticidin. HT1080-GPX4/FSP1^{DKO} cells were generated by infecting HT1080-GPX4^{KO}-Cas9 cells with sgAIFM2 lentivirus (Sigma #HS5000029901) and selecting with 2μg/ml puromycin. HT1080-GPX4/SCD1^{DKO} cells were generated by infecting HT1080-GPX4^{KO}-Cas9 cells with sgSCD lentivirus (Sigma # HS5000004019) and selecting with 2μg/ml puromycin. HT1080-GPX4^{KO}-Cas9-SCD1/gMBOAT2 cells were generated by infecting HT1080-GPX4^{KO}-Cas9-SCD1cells with sgMBOAT2 lentivirus (Sigma # HS5000029185 and # HS5000029186) and sorting of BFP+ cells by FACS. HT1080-GPX4^{KO} cells and their derived cell lines were maintained with 100μM Trolox in the medium.

LnAR-iCas9 cells were generated by transiently transfecting LnAR cells with pAAVS1-tet-iCas9-BFP2 (Addgene #125519) and AAVS1 T2 CRIPR in pX330 (Addgene #72833) by Lipofectamine 3000 reagent. After transfection, cells were treated with 1 μg/ml Dox for 48h and sorted BFP+ cells by FACS. LnAR-igGPX4 cells were generated by infecting LnAR-iCas9 cells with sgGPX4-puro (TGATCTCTTCGTTACTCCCTGG; Sigma # HS5000001523) and sgGPX4-blast (CACGCCCGATACGCTGAGTG) lentivirus simultaneously and selecting with 2 μg/ml puromycin and 20μg/ml Blasticidin in Tetracycline free medium. GPX4 knockout was induced by treated LnAR-igGPX4 with 1 μg/ml Dox for at least 4 days. LnAR-gMBOAT2 cells were generated by infecting LnAR-iCas9 cells with sgMBOAT2#1 (CTTTGTACAAGAAAGTGTAAGG; Sigma # HS5000029185) or sgMBOAT2#2 (TACTGCTTTGTGTTTGCTCTGG; Sigma # HS5000029186) lentivirus respectively and selecting with 2 μg/ml puromycin and 1 μg/ml Dox. T47D-gMBOAT1 cells were generated by infecting T47D-Cas9 cells with sgMBOAT1#1 (TCTGTGCATCTTTTTGTGCTGG; Sigma # HS5000018673) and sgMBOAT1#2 (TCTGAGTGACAATCATCAGAGG; Sigma # HS5000018674) lentivirus simultaneously and selecting with 2 μg/ml puromycin.

Generation of shRNA expression cells

shMBOAT2 cells were generated by infecting HT1080, SUIT-2, LNCaP and LnAR cells with indicated shMBOAT2 lentiviruses (#1: TRCN0000035240; #2: TRCN0000370550) and selecting with 2μg/ml puromycin. Inducible shMBOAT2 cells were generated by infecting indicated cells with LT3G-ishMBOAT2 and sorting of GFP^{+} cells. shACSL3 cells were generated by infecting HT1080-GPX4^{KO} -MBOAT2 cells with indicated shACLS3 lentiviruses (#1: TRCN0000045530; #2: TRCN0000045532) and selecting with 2 μg/ml puromycin. shFOXA1 cells were generated by infecting indicated cells with shFOXA1 lentiviruses (#1: Addgene 70095; #2: Addgene

70096) and selecting with 2 μg/ml puromycin. ishAR cells were generated by infecting indicated cells with LT3G-ishAR and sorting of GFP$^+$ cells. shMBOAT1 cells were generated by infecting indicated cells with shMBOAT1lentiviruses (TRCN0000035315). shNT cells were generated by infecting indicated cells with shNT lentiviruses (Sigma #SHC016).

Generation of stable expression cells

To generate MBOAT1, MBOAT2, MBOAT5, MBOAT7, LPCAT4, DGAT1, PLA2G2F, SCD, ACSL3, FSP1 and AR overexpression cells, indicated cells were infected with retroviruses and selected by either 2 μg/ml puromycin, 20 μg/ml Blasticidin or sorting of mCherry$^+$ cells. To generate NOS2 overexpression cells, indicated cells were infected with pLIX403-hNOS2 (Addgene #110800) lentiviruses; to generate GCH1 overexpression cells, indicated cells were infected with GCH1_pLX307 lentiviruses (Addgene #98336). Cells were selected with 2 μg/ml puromycin.

CRISPR activation screen and data analysis

HT1080-dCas9 cells were established by infection of HT1080 cells with dCAS9_VP64_Blast lentiviral particles (Addgene 61425-LV) and selection with 20 μg/ml Blasticidin. HT1080-dCas9/CRISPRa library cells were established by infection of HT1080-dCas9 cells with Human CRISPRa sgRNA library Calabrese Set A concentrated lentiviral particles[56] (Addgene 92379-LVC) and selection with puromycin following Addgene's protocol (https://www.addgene.org/pooled-library/broadgpp-human-crispra-calabrese-p65hsf/). Briefly, 4.5×10^7 cells were infected at 50% infection efficiency to achieve a representation of ~400 cells per sgRNA. Puromycin selected library cells were then expanded for one passage to total 1.0×10^8 cells. For control, 2.0×10^7 cells were harvested at day 0; for screening, 8.0×10^7 cells were equally seeded in 40 dishes (10-cm). The next day, screen cells were treated with 0.1 μM RSL3 (10 dishes × 2 replicates) or cystine starvation medium (10 dishes × 2 replicates). 24 h post treatment, fresh normal medium was replaced. At this time, >98% cells were dead from ferroptosis, and only <2% cells were survived. The recovered cells were pooled together, expanded, and subjected to second round of screening. After two rounds of selection, the ferroptosis resistant cells were harvested for sequencing (~2.0×10^7 cells of each replicate were collected).

Cellular DNA was extracted by Blood and Cell Culture DNA Midi Kit (Qiagen), and the sgRNA fragments were amplified by Ex Taq DNA polymerase (Clontech) with Guide-F primer: TTGTGGAAAGGACGAAACACCG and Guide-R primer: TCTACTATTCTTTCCC CTGCACTGT, and purified with AMPure XP reagent followed Addgene's protocol. The amplified DNAs were subjected to amplicon sequencing (PE100, ~30 M reads for each sample) at the Integrated Genomics Operation (IGO) core of MSKCC.

Clean reads were obtained by filtering raw sequence file (FASTQs) to remove adapter sequences and low-quality bases with custom scripts, and were then analyzed with Model-based Analysis of Genome-wide CRISPR-Cas9 Knockout (MAGeCK) (version 0.5.9).[59] Read counts were initially obtained from individual samples with the count command in MAGeCK, in which the software fastqc was used to assess the quality of the sequencing data and reads from high-quality samples were further mapped to the screening library. The top positively selected and negatively selected sgRNAs were identified with the test command in MAGeCK, and in this process, read counts were normalized on the basis of total count normalization to exclude the effect of sequencing depth. The robust rank aggregation (α-RRA) algorithm was then used to calculate the RRA score, which reflects the degree of positive or negative selection. Associated plots were created using R package ggplot2 (https://ggplot2.tidyverse.org).

3′-RNA Quant-seq and data analysis

Cells (1×10^6 per treatment condition) were lysed in 350 μl of Buffer RLT plus, and total RNA was extracted from cell pellets using RNeasy Plus Mini kit (Qiagen, 74134) following manufacturer protocol. RNA yield and quality were assessed using the 2200 TapeStation (Agilent). Sequencing libraries were prepared using the QuantSeq 3′-mRNA Seq Library Prep Kit FWD for Illumina (Lexogen, SKU: 015.96) from 500 ng of total RNA spiked with ERCC RNA Spike-In Mix 1 (1:1000, Thermofisher Scientific, 4456740). Briefly, first-strand (oligo(dT)) cDNA synthesis was followed by RNA removal and second-strand synthesis via random priming. The double-stranded library was bead purified to remove reaction components before PCR amplification with i7 single-index primers for 8 cycles. Amplified libraries were again bead purified according to the manufacturer's protocol, and concentration was measured by Qubit assay. All samples were checked for fragment size distribution on Tapestation before pooling for 50 base-pair single-end reads were sequencing on the Illumina NextSeq 550 platform.

Gene and 3' UTR annotations were obtained from the UCSC table browser (https://genome.ucsc.edu/cgi-bin/hgTables, hg38). Adapters were trimmed from raw reads using cutadapt through the trim_galore wrapper tool with adapter overlaps set to 3 bp for trimming. For Quant-seq, concatenated fastq files were trimmed for adaptor sequence, and masked for low-complexity or low-quality sequence using trim_galore, then mapped to hg38 whole genome using HISAT 2.2.1 with default parameters.[65] The number of reads mapped to the 3' UTR of genes was determined with featureCounts.[66] Raw reads were normalized to counts per million (CPM). Analysis of differential gene expression was restricted to genes with ≥ 10 reads in at least one condition. Differential gene expression calling was performed on raw read counts using DESeq2 with default settings. Downstream analysis was restricted to genes passing all internal filters for FDR estimation by DESeq2.[67] Plots of differential gene expression were visualized using ggplot2 package in R with significant genes (Adjusted P value <0.01, $|\log_2 FC| \geq 1$).

LIPIDOMIC ANALYSES

Sample preparation

5×10^6 HT1080-Vec, HT1080-MBOAT1, HT1080-MBOAT2, LnAR-shNT, LnAR-ishMBOAT2, T47D-Cas9, or T47D-gMBOAT1 cells (5 replicates for each cell type) were harvested by scraping the cells in 3 ml cold PBS (containing 0.001% W/V butylated hydroxytoluene, BHT). LnAR-shNT and LnAR-ishMBOAT2 cells were treated with 1 μg/ml Dox for 48 h to induce MBOAT2 knockdown before harvest. An aliquot of cells was retained to determine protein concentration (BCA assay). The remaining cells were pelleted down and snap frozen in liquid nitrogen. The frozen cell pellets were sent to Mass Spectrometry Core Facility of Columbia University for lipidomic analysis. Briefly, lipid was extracted by homogenizing the cell pellets with 250 μl cold methanol containing 0.01% BHT and 1 μl of SPLASH lipidomics internal standard mix (Avanti Polar Lipids) by a microtip ultrasonic homogenizer. Cell lysates were then transferred into a pre-chilled glass vial with a Teflon-lined cap. 850 μl ice-cold methyl tert-butyl ether (MTBE) was added and the glass vial was vigorously vortex-mixed for 30s. The samples were incubated on ice for 2 h on the shaker, followed with the addition of 200 μl ice-cold water. The samples were incubated for 20 min on ice and centrifuged at 3,500 r.p.m. for 20 min at 4 °C to achieve phase separation. The top layer containing the lipids was transferred to a separate pre-chilled glass vial and dried under a gentle nitrogen stream. The dried samples were reconstituted with 2-propanol/acetonitrile/water (4:3:1, v/v/v and 0.01% butylated hydroxytoluene) before LC–MS analysis. A quality control sample was prepared by combining 50 μl of each sample to assess the reproducibility of the features through the runs.

LC conditions

Lipids were separated using an Acquity UPLC CSH column (2.1 × 100 mm, 1.7 μm) over a 20-min gradient elution on a Waters Acquity UPLC I-Class system. Mobile phase A consisted of acetonitrile/water (60:40, v/v) and mobile phase B was 2-propanol/acetonitrile/water (85:10:5, v/v/v) both containing 10 mM ammonium acetate and 0.1% acetic acid. After the injection, the gradient was held at 40% mobile phase B for 2 min. At 2.1 min, it reached to 50% B, then increased to 70% B in 12 min, at 12.1 min changed to 70% B and at 18 min increased to 90% B. The eluent composition returned to the initial condition in 1 min, and the column was re-equilibrated for an additional 1 min before the next injection was conducted. The oven temperature was set at 55 °C and the flow rate was 400 μl min^{-1}. The injection volume was 6 μl using the flow-through needle mode. The quality control sample was injected between the samples and at the beginning and end of the run to monitor the performance and the stability of the MS platform.

MS conditions

The SYNAPT G2-Si -Q-ToF mass spectrometer was operated in both positive and negative electrospray ionization modes. For the positive mode, a capillary voltage and sampling cone voltage of 2 kV and 32 V were used. The source and desolvation temperatures were kept at 120 and 500 °C, respectively. Nitrogen was used as the desolvation gas with a flow rate of 800 l h^{-1}. For the negative mode, a capillary voltage of 1.5 kV and a cone voltage of 30 V were used. The source temperature was 120 °C and the desolvation gas flow was set to 800 l h^{-1}. Depending on the ionization mode, the protonated molecular ion of leucine encephalin ($[M + H]^+$ mass to charge ratio (*m/z*): 556.2771) or the deprotonated molecular ion ($[M - H]^-$, *m/z*: 554.2615) was used as a lock mass for mass accuracy and reproducibility. The data were collected in duplicates in data-independent (MS^E) mode over the mass range m/z: 50 to 1,200 Da. The quality control sample was also acquired in enhanced data-independent ion mobility (HDMSE) in both positive and negative modes for enhancing the structural assignment of lipid species. The electrospray ionization source settings for ion mobility were the same as described above. The travelling wave velocity was set to 650 m s^{-1} and the wave height was 40 V. The helium gas flow in the helium cell region of the ion-mobility spectrometry cell was set to 180 ml min^{-1}. Nitrogen, used as the drift gas, was held at a flow rate of 90 ml min^{-1} in the ion-mobility spectrometry cell. The low collision energy was set to 4 eV and the high collision energy was ramped from 25 to 60 eV in the transfer region of the T-Wave device to induce the fragmentation of mobility-separated precursor ions.

Data preprocessing and statistical analysis

All raw data files were processed in Progenesis QI software. Multivariate and univariate statistical analyses were performed using MetaboAnalyst 4.0[68] and also in an R environment. The signal intensity of each ion was then normalized to the measured protein concentrations. Group differences were calculated using either a two-tailed parametric Welch's *t* test with a fold-change threshold of 1.5 (average signal intensities of treated over average signal intensities of vehicle groups) or one-way ANOVA. *P* values were corrected for multiple hypothesis testing and an FDR of 0.05 or less was considered significant.

Structural assignment of identified lipids

The structural elucidation and validation of significant features were initially obtained by searching monoisotopic masses against the Lipid MAPS database[69] with a mass tolerance of 5 ppm. Fragment ion information obtained by tandem MS (UPLC–HDMSE) was used for the further structural elucidation of significantly changed lipid species. HDMSE data were processed using MS^E data viewer (version 1.3, Waters Corp.).

Please cite this article in press as: Liang et al., Ferroptosis surveillance independent of GPX4 and differentially regulated by sex hormones, Cell (2023), https://doi.org/10.1016/j.cell.2023.05.003

Chromatin immunoprecipitation (ChIP)

ChIP experiments were carried out according to standard protocols.[70] The cells were fixed with 1% formaldehyde for 10 min, after which the reaction was quenched by the addition of glycine to the final concentration of 0.125 M. The fixed cells were washed with PBS and resuspended in SDS buffer (100 mM NaCl, 50 mM Tris-HCl pH 8.0, 5 mM EDTA, 0.5% SDS, 1× protease inhibitor cocktail). The resulting nuclei were spun down, resuspended in the immunoprecipitation buffer at 1 mL per 16 million cells (SDS buffer and Triton Dilution buffer (100 mM NaCl, 100 mM Tris-HCl pH 8.0, 5 mM EDTA, 5% Triton X-100) mixed in 2:1 ratio with the addition of 1× protease inhibitor cocktail from Roche) and processed on a Bioruptor Plus Sonicator (Diagenode) to achieve an average fragment length of 200-300 bps. The immunoprecipitation reactions were set up in 1 mL of the immunoprecipitation buffer as indicated below and incubated overnight at 4 °C. The next day, BSA-blocked Protein G Dynabeads were added to the reactions and incubated for 3 hours at 4 °C. The beads were then washed three times with low-salt washing buffer (150 mM NaCl, 1% Triton X-100, 0.1% SDS, 2 mM EDTA, 20 mM Tris-HCl pH8.0) and two times with high-salt washing buffer (500 mM NaCl, 1% Triton X-100, 0.1% SDS, 2 mM EDTA, 20 mM Tris-HCl pH8.0). Beads were incubated in elution buffer (100 mM $NaHCO_3$, 1% SDS) overnight at 65 °C shaking at 800 rpm for de-crosslinking. De-crosslinked DNA was purified using the Qiagen PCR Purification kit. qPCR analysis was carried out on ChIPed and input DNA (primer sequences in key resources table). Data are presented as percent of input DNA, and error bars represent s.d. for technical duplicates of the qPCR analysis.

Generating of drug resistant breast cancer cells

MCF7/T47D fulvestrant resistant cells were generated by treating cells with fulvestrant from 100 nM to 400 nM for two months (concentration increased gradually) and maintained in media containing 400 nM fulvestrant afterwards. MCF7 tamoxifen resistant cells were generated by treating with 4OHT from 500 nM to 2 μM for two months (concentration increased gradually) and maintained in media containing 1 μM 4OHT afterwards. Parental cells were cultured in the meantime and used as control.

Cell death assay

Cells were seeded at an appropriate cell density and cultured in normal condition for 24h. Cells were then stained with Hoechst 33342 (0.1μg/mL) for 20 min followed by indicated treatments as described in individual experiments with Sytox green (5 nM) to monitor cell death. Culture plates were read by Cytation5 at indicated time points. Percentage of cell death was calculated as Sytox green$^+$ cell number over Hoechst 33342$^+$ cell number.

Cell viability assay

Cells were seeded at appropriate cell density and subjected to indicated treatments as described in individual experiments. At the end of treatment, cell viability was measured by CellTiter-Glo Luminescent Cell Viability Assay (Promega) following the manufacturer's instructions. Relative viability was calculated by normalizing ATP levels of treatments to no treatment control.

Measurement of Lipid Peroxidation

Cells were seeded at appropriate density and subjected to indicated treatment followed by BODIPY C11(5 μM; Thermo Fisher #D3861) staining for 30 min. Labeled cells were then trypsinized, resuspended in PBS plus 2% FBS, and subjected to flow cytometry analysis. Oxidation of BODIPY C11 resulted in a shift of the fluorescence emission peak from 590 nm to 510 nm.

Western Blot

Cells were harvested and lysed by RIPA buffer. For MBOAT1/2 western blot, cell lysates were not subjected to boiling to avoid protein aggregation, otherwise, cell lysates were boiled and resolved on SDS/PAGE gels and transferred to a nitrocellulose membrane. The membranes were blocked in 5% skim milk for 1 h at room temperature and then incubated with indicated diluted primary antibodies at 4 °C overnight. After three washes with TBST, membranes were incubated with goat anti-mouse HRP-conjugated antibody or donkey anti-rabbit HRP-conjugated antibody (Invitrogen) for 1 h at room temperature. After three washes with TBST, membranes were developed by Clarity Western ECL Substrate (Bio-Rad) and imaged by Amersham Imager 600 (GE Healthcare Life Sciences).

qRT-PCR

Cells were lysed by Trizol solution (Invitrogen) after indicated treatments. Total RNA was extracted following manufacturer's instructions. cDNAs were synthesized by iScript Reverse Transcription Supermix (Bio-Rad). qPCR was performed using IQ™ SYBR® Green Supermix reagents (Bio-Rad). GAPDH was used as the internal control. The relative expression of indicated genes was calculated by ΔΔ CT method.

Animal Models

To create the prostate cancer xenograft mouse model, LnAR-igGPX4 cells were subcutaneously (S.C.) inoculated into the right flank of 5-6 weeks old male athymic nu/nu mice (Charles River Laboratories, Wilmington, MA) by injecting 1×10^7 cells in 50% matrigel. The maximum width (X) and length (Y) of the tumor were measured by caliper every two days and the volume (V) was calculated using the formula: $V = (X^2Y)/2$. Once tumors were palpable (~250 mm^3), mice were randomly placed into four groups: 1) Vehicle group daily intraperitoneal (i.p.) with vehicle (65% D5W (5% dextrose in water), 5% Tween-80 and 30% PEG-400) and normal diet; 2)

Please cite this article in press as: Liang et al., Ferroptosis surveillance independent of GPX4 and differentially regulated by sex hormones, Cell (2023), https://doi.org/10.1016/j.cell.2023.05.003

Enzalutamide (ENZ, MedchemExpress) group daily i.p. with 10 mg/kg ENZ dissolved in vehicle and normal diet; 3) Doxycycline (DOX) group daily i.p. with vehicle and with DOX diet (625 ppm, ENVIGO); 4) ENZ + DOX group daily i.p. with 10 mg/kg ENZ and DOX diet. Mice were given i.p. injections of 0.9% sterile saline or DOX (100 mg/kg body weight) for 2 days before ENZ treatment. 15 days post-treatments, mice were euthanized with CO_2 and tumors were dissected for weight, histological and immunostaining analysis.

To construct the orthotopic breast cancer mouse model, female NOD/SCID mice (ENVIGO), aged 5-6 weeks, were S.C. implanted with 17-β-estradiol 90-d release pellets (0.72mg, Innovative Research of America) 3 days before tumor inoculations. Then, 1×10^7 MCF7-FulR$^+$ cells in 50% Matrigel were injected into the mammary fat pad of the anesthetized mice. Tumor sizes were measured by caliper every two days and calculated as described above. Once tumors were palpable (~250 mm^3), mice were randomly divided into 4 groups: 1) Vehicle group daily i.p. with vehicle (65% D5W (5% dextrose in water), 5% Tween-80, 30% PEG-400), 2) Fulvestrant (Ful) group weekly S.C. with Ful 5 mg (Sandoz Inc., Cat: NDC 0781-3492-12), 3) IKE group daily i.p. with 40 mg/kg IKE (MedchemExpress) dissolved in vehicle; 4) Ful + IKE group weekly S.C. with Ful 5 mg and daily i.p. with 40 mg/kg IKE. 15 days post-treatments, mice were euthanized with CO_2 and tumors were dissected for weight, histological and immunostaining analysis.

All protocols for animal experiments were approved by the Memorial Sloan Kettering Cancer Center Institutional Animal Care and Use Committee (IACUC).

Immunohistochemistry

Antigen retrieval was performed with the Retrievagen A antigen retrieval system (550524, BD Biosciences) following manufacturer's instructions. Immunohistochemical staining was performed using anti-mouse/rabbit HRP-DAB Cell & Tissue Staining Kit (R&D Systems) following manufacturer's instructions. Primary antibody used for the staining were listed in key resources table.

QUANTIFICATION AND STATISTICAL ANALYSIS

Please refer to the legend of the figures for description of sample sizes and statistical tests performed. Data were plotted and analyzed with GraphPad Prism 9.0 software. Differences were considered statistically significant when the p-value was less than 0.05, and otherwise not significant (ns). Illustrations were prepared using Adobe Illustrator and BioRender (BioRender.com).

CellPress

Supplemental figures

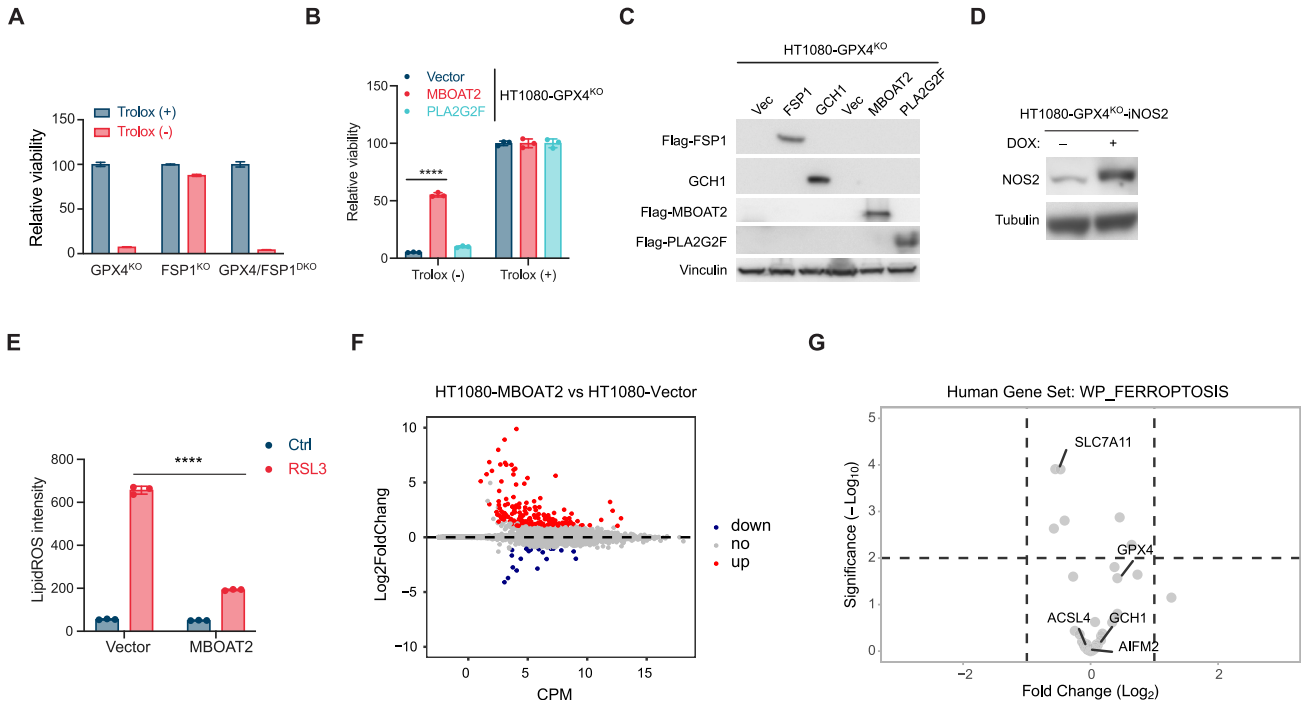

Figure S1. MBOAT2 is a GPX4/FSP1-independent ferroptosis suppressor, related to Figure 1

(A) Viability analysis of HT1080-GPX4^{KO}, HT1080- FSP1^{KO}, and HT1080-GPX4/FSP1^{DKO} cells cultured with or without 100 μM trolox as indicated for 24 h. Data are presented as mean ± SD (n = 3 biologically independent samples).

(B) Viability analysis of HT1080-GPX4^{KO} cells expressing vector control, MBOAT2, and PLA2G2F. Cells were cultured with or without 100 μM trolox as indicated for 24 h. Data are presented as mean ± SD (n = 3 biologically independent samples).

(C) Western blot analysis confirming overexpression of indicated genes in HT1080-GPX4^{KO} cells.

(D) Western blot analysis confirming Dox-inducible NOS2 expression in HT1080-GPX4^{KO} cells. Cells were treated with 1 μg/mL Dox for 48 h.

(E) Quantification of lipid peroxidation in HT1080 cells with or without MBOAT2 overexpression as indicated. Cells were treated with 0.1 μM RSL3 for 3 h prior to labeling with BODIPY-C11.

(F) RNA-seq analysis identified genes upregulated (red) or downregulated (blue) by MBOAT2 overexpression in HT1080 cells.

(G) Volcano plot showing the differential expression of ferroptosis-related genes (WikiPathways_ferroptosis) in HT1080 cells expressing MBOAT2 vs. vector control. A cohort of ferroptosis regulatory genes are shown without significant change of expression. See also Table S1.

Statistical analysis was performed using one-way ANOVA (B) or two-tailed t test (E). ****p < 0.0001.

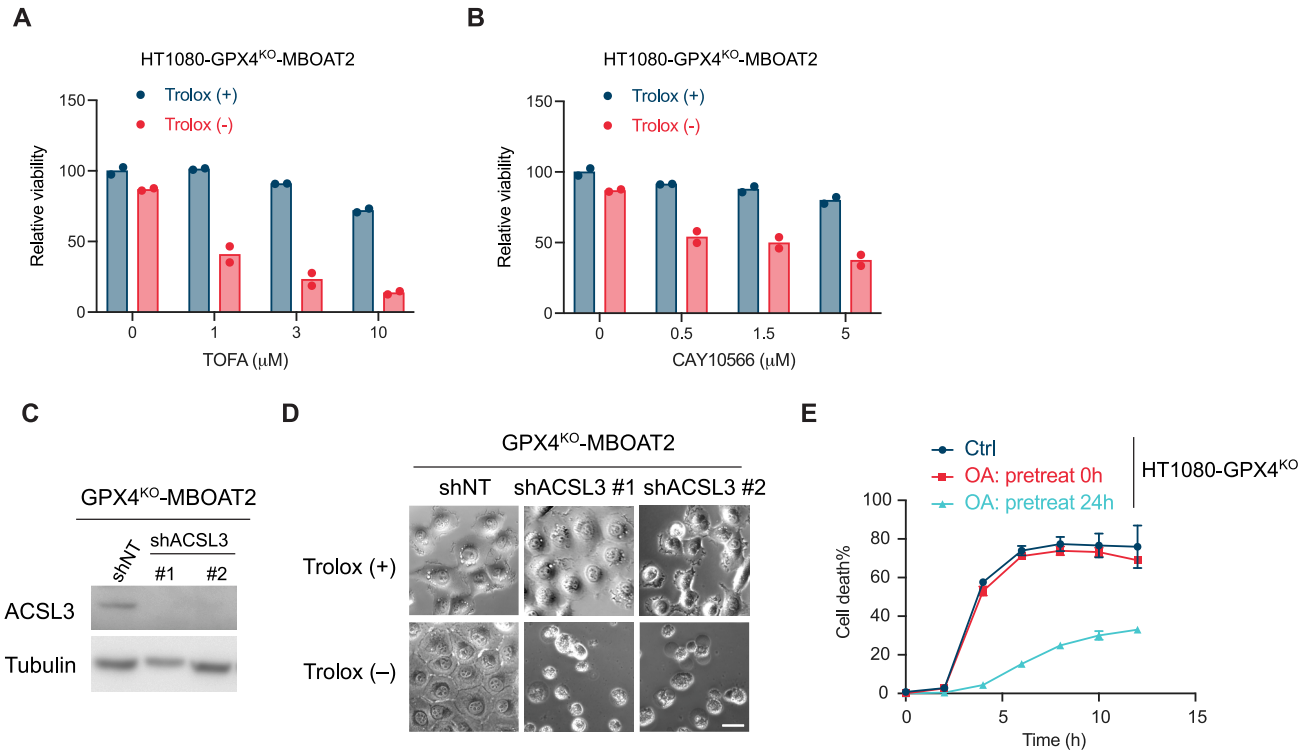

Figure S2. The ferroptosis-suppressing function of MBOAT2 requires either endogenous or exogenous MUFA, related to Figure 2

(A and B) Viability analysis of HT1080-GPX4^{KO} cells overexpressing MBOAT2. Cells were treated with indicated concentration of TOFA (A) or CAY10566 (B), in the presence or absence of trolox as indicated for 48 h. n = 2 biologically independent samples.

(C) Western blot analysis confirming ACSL3 shRNA knockdown in HT1080-GPX4^{KO} cells overexpressing MBOAT2.

(D) Images showing viability of cells with indicated genetic background. Cells were cultured with or without trolox as indicated for 24 h. Scale bars, 10 μM. Two independent experiments were performed, and representative images from one experiment are shown.

(E) Cell death time course of HT1080-GPX4^{KO} cells. Cells were either mock treated or pretreated with 10 μM OA for indicated time before removing trolox to initiate ferroptosis. Data are presented as mean ± SD (n = 3 biologically independent samples).

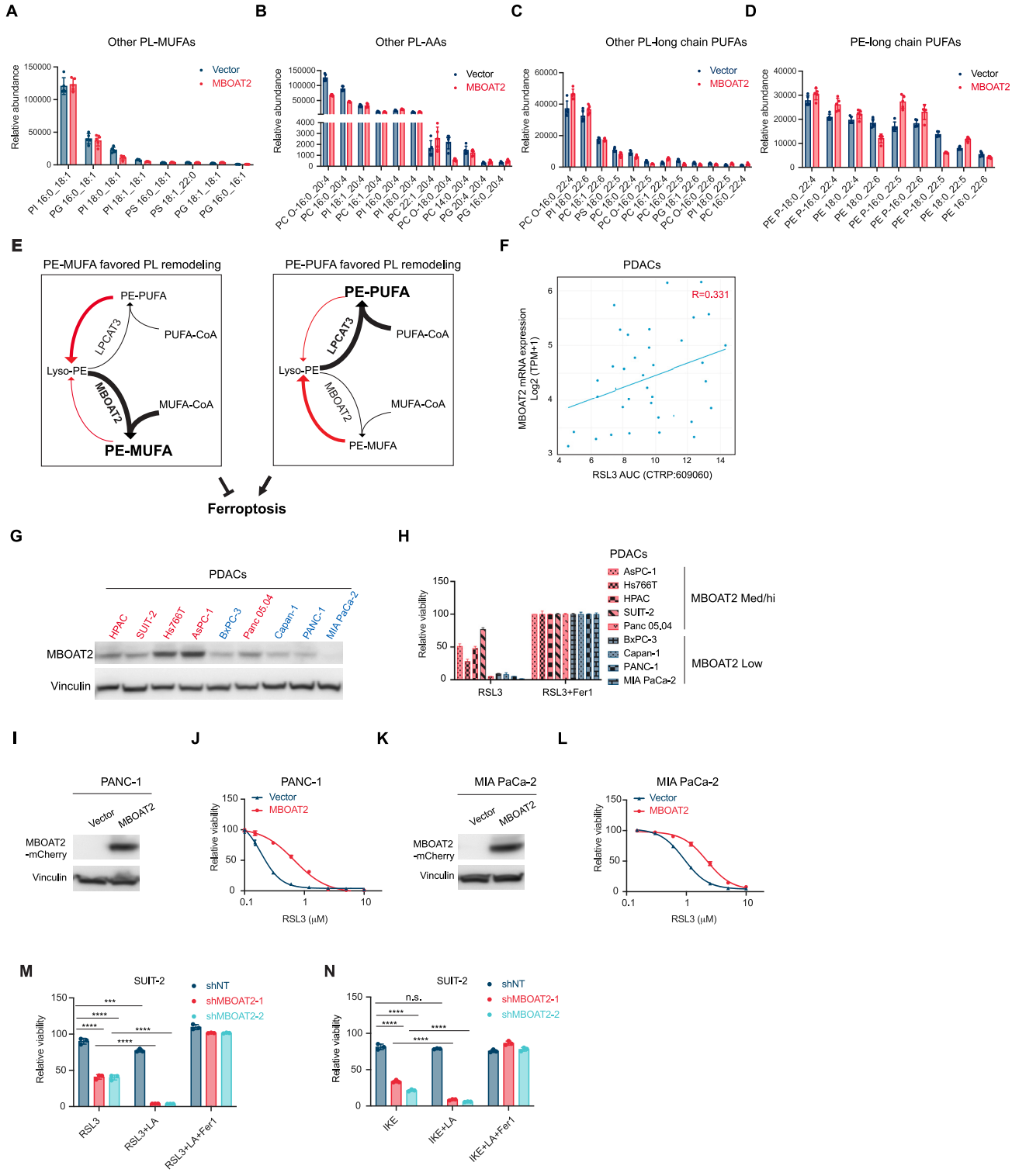

Figure S3. MBOAT2 suppresses ferroptosis through phospholipid remodeling, related to Figure 3

(A–D) Quantification of abundant PLs other than those described in Figures 3A–3D as following: PL-MUFAs (A), PL-AAs (B), PL-long chain PUFAs (C) and PE-long chain PUFAs (D) in HT1080 cells expressing vector control or MBOAT2 as indicated. Data are presented as mean ± SD (n = 5 biological replicates).

(E) A working model depicting that MBOAT2 suppresses ferroptosis through PL remodeling. As a lyso-PE acyltrasferase (LPEAT) with MUFA preference, MBOAT2 competes with LPEATs with PUFA preference (e.g., LPCAT3). When MBOAT2 activity is dominant, cells have a high PE-MUFA/PE-PUFA ratio and

(legend continued on next page)

therefore are more resistant to ferroptosis. Conversely, if LPCAT3 activity is dominant, cellular lipidome will be remodeled toward a low PE-MUFA/PE-PUFA ratio, thus more sensitive to ferroptosis.

(F) Correlation of MBOAT2 mRNA level and RSL3 resistance score in PDAC lines (adapted from DepMap portal). R = 0.331, Pearson correlation.

(G) Western blot analysis showing endogenous MBOAT2 expression in a panel of PDAC lines.

(H) Viability analysis of a panel of PDAC lines. Ferroptosis was induced by 1 μM RSL3 for 24 h, in the absence or presence of 10 μM Fer1 as indicated. Data are presented as mean ± SD (n = 3 biological independent samples).

(I and K) Western analysis showing overexpression of ectopic MBOAT2 in PANC-1 and MIA PaCa-2 cells.

(J and L) Viability analysis of PANC1 and MIA PaCa-2 cells harboring vector control or MBOAT2 overexpression. Ferroptosis was induced by indicated concentration of RSL3 for 24 h.

(M and N) Viability analysis of SUIT-2 cells expressing control or MBOAT2 shRNA. As indicated, cells were pretreated with or without adding 10 μM linoleic acid (LA) to culture medium for 24 h, and then ferroptosis was induced by 1 μM RSL3 (M) or 1 μM IKE (N), in the presence or absence of Fer1, for another 24 h. Data are presented as mean ± SD (n = 3 biologically independent samples). Statistical analysis was performed using one-way ANOVA (M and N). *$p < 0.05$, **$p < 0.01$, ***$p < 0.001$, ****$p < 0.0001$.

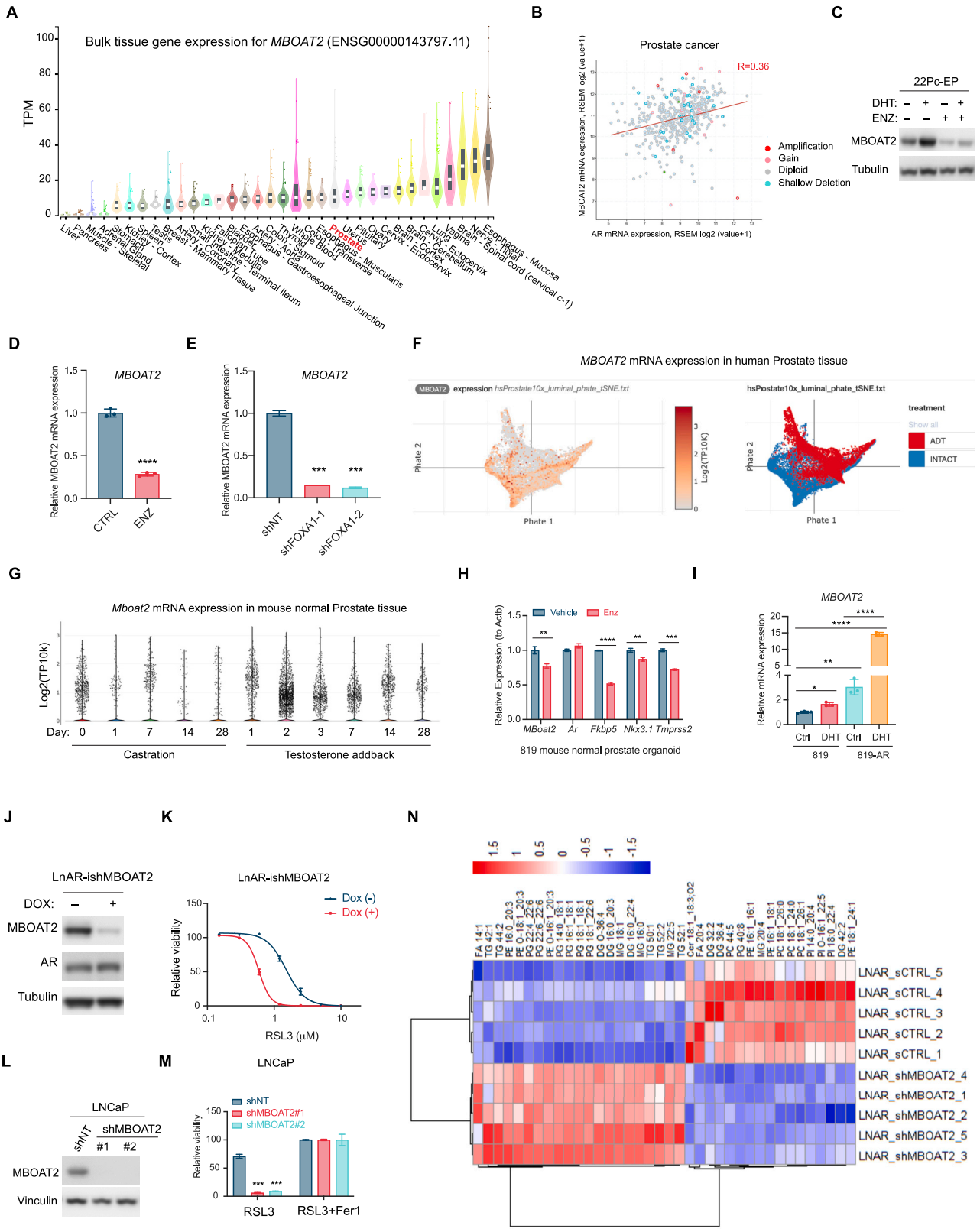

(legend on next page)

Figure S4. AR signaling modulates ferroptosis sensitivity in prostate cancer cells through MBOAT2, related to Figure 4

(A) *MBOAT2* mRNA expression in normal human tissues (adapted from GTEx Portal). Expression levels are shown in TPM (transcripts per million). Boxplots are shown as median and 25th and 75th percentiles.

(B) Correlation of *MBOAT2* mRNA level and *AR* mRNA level in human prostate cancer samples (TCGA PanCancer Atlas Studies, cBioportal). mRNA level was batch normalized from Illumina HiSeq_RNASeqV2 and shown as $\log_2$(RSEM + 1). R = 0.36, Spearman correlation.

(C) Western blot analysis showing MBOAT2 expression in 22Pc-EP prostate cancer cells with indicated treatment for 48 h. DHT: 100 nM; ENZ: 5 μM.

(D) qRT-PCR analysis showing relative *MBOAT2* mRNA level in LNCaP cells that were treated with either DMSO control or 5 μM ENZ for 48 h. Data are presented as mean ± SD (n = 3 biological independent samples).

(E) qRT-PCR analysis showing relative *MBOAT2* mRNA level in LnAR-shNT and LnAR-shFOXA1 cells. Data are presented as mean ± SD (n = 3 biologically independent samples).

(F) Left: PHATE maps colored by MBOAT2 mRNA level; right: PHATE map of luminal cells from all samples stratified by treatment. Data adapted from Single-cell portal (https://singlecell.broadinstitute.org/single_cell/study/SCP864).

(G) Single-cell *MBOAT2* mRNA expression in normal mouse prostate tissues after castration and androgen addback. Data adapted from Single-cell portal (https://singlecell.broadinstitute.org/single_cell/study/SCP859).

(H) mRNA expression of multiple AR target genes was detected by qRT-PCR in 819 mouse normal prostate organoid treated with DMSO control (Ctrl) or 10 μM ENZ for 48 h. Data are presented as mean ± SD (n=3 biologically independent samples).

(I) *MBOAT2* mRNA expression was detected by qRT-PCR in 819 and 819-AR cells mouse normal prostate organoid treated with 100 nM DHT for 24 h. Data are presented as mean ± SD (n=3 biologically independent samples).

(J) Western blot analysis confirming Dox-inducible shRNA knockdown of MBOAT2 in LnAR-ishMBOAT2 cells. Dox treatment: 1 μg/mL for 48 h.

(K) Viability analysis of LnAR-ishMBOAT2 cells. Cells were preincubated with or without 1 μg/mL Dox for 48 has indicated, followed by ferroptosis induction with indicated concentration of RSL3 for 24 h. Data are presented as mean ± SD (n = 3 biological independent samples).

(L) Western blot analysis confirming MBOAT2 knockdown in LNCaP-shMBOAT2 cells.

(M) Viability analysis of indicated cells treated with RSL3 (1 μM) in the absence or presence of Fer1 (10 μM) as indicated for 24 h. Data are presented as mean ± SD (n = 3 biologically independent samples).

(N) Heatmap of lipid species that were significantly changed between LnAR-NT and LnAR-shMBOAT2 cells. Two-tailed t test, FDR-corrected p value < 0.05, fold change threshold = 1.5.

Statistical analysis was performed using one-way ANOVA (E, I, and M) or two-tailed t test (D and H). **p < 0.01, ***p < 0.001, ****p < 0.0001.

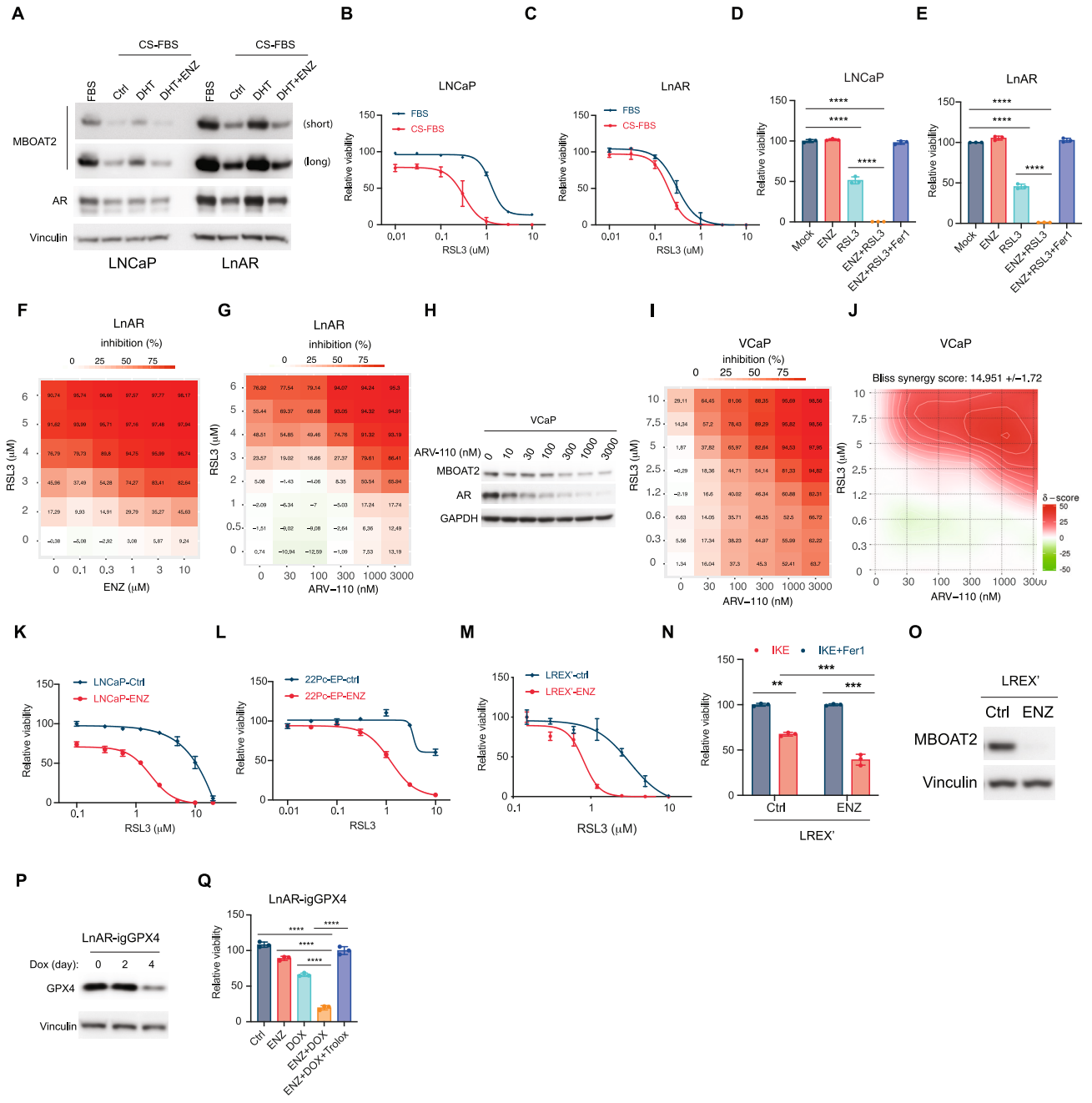

Figure S5. AR antagonist sensitizes AR$^+$ prostate cancer cells to ferroptosis *in vitro* and *in vivo*, related to Figure 5

(A) Western blot analysis showing MBOAT2 and AR expression in LNCaP and LnAR cells cultured either in medium containing 10% normal FBS or in medium containing 10% charcoal-stripped FBS (CS-FBS), followed by indicated treatments for 48 h. ENZ: 5 μM; DHT: 100 nM.

(B and C) Viability analysis of LNCaP (B) and LnAR (C) cells cultured either in medium containing 10% normal FBS or in medium containing10% CS- FBS for 48 h, followed by ferroptosis induction with indicated concentration of RSL3 for 24 h. Data are presented as mean ± SD (n = 3 biologically independent samples).

(D and E) Viability analysis of LNCaP (D) and LnAR (E) cells with indicated treatment. Cells were pretreated either with DMSO or 5 μM ENZ for 48 h, followed by RSL3 (3 μM) in the presence or absence of Fer1 (10 μM) for another 24 h. Data are presented as mean ± SD (n = 3 biologically independent samples).

(F and G) Dose-response matrix (B) of LnAR cells following treatment with a combination of ENZ and RSL3 (F) or ARV-110 and RSL3 (G). Matrix was generated by SynergyFinder 3.0 (https://synergyfinder.fimm.fi/).

(H) Western blot analysis showing MBOAT2 and AR expression in VCaP prostate cancer cells with indicated treatment for 48 h.

(I and J) Dose-response matrix (I) and Bliss synergy score surface plots (J) of VCaP cells with a combination of ARV-110 and RSL3 treatment. Cells were pre-treated with indicated ARV-110 for 48 h, followed by treatment with indicated concentration of RSL3 for 24 h. Synergy scores and plots were generated by SynergyFinder 3.0 (https://synergyfinder.fimm.fi/).

(legend continued on next page)

(K–M) Viability analysis of LNCaP (K), 22Pc-EP (L), and LERX' (M) cells. Cells were pretreated with DMSO vehicle control or 5 μM ENZ for 48 h, followed by ferroptosis induction with indicated concentration of RSL3 for 24 h. Data are presented as mean ± SD (n = 3 biologically independent samples).
(N) Viability analysis of LREX' cells with or without pretreatment of 5 μM ENZ for 48 h, as indicated. Ferroptosis was induced by 10 μM IKE for 24 h, in the absence or presence of 10 μM Fer1 as indicated. Data are presented as mean ± SD (n = 3 biologically independent samples).
(O) Western blot analysis showing MBOAT2 expression in LREX' cells in response of the treatment of 1 μM ENZ for 48 h.
(P) Western blot analysis showing GPX4 expression in LnAR cells harboring Dox-inducible GPX4 knockout (LnAR-igGPX4) treated with 1 μg/mL Dox for 0, 2, or 4 days as indicated.
(Q) Viability analysis of LnAR-igGPX4 cells with indicated treatment for 7 days. ENZ: 1 μM; Dox: 1 μg/mL; trolox: 100 μM. Data are presented as mean ± SD (n = 3 biologically independent samples).
Statistical analysis was performed using one-way ANOVA (D and E) or two-tailed t test (N). $^{**}p < 0.01$, $^{***}p < 0.001$, $^{****}p < 0.0001$.

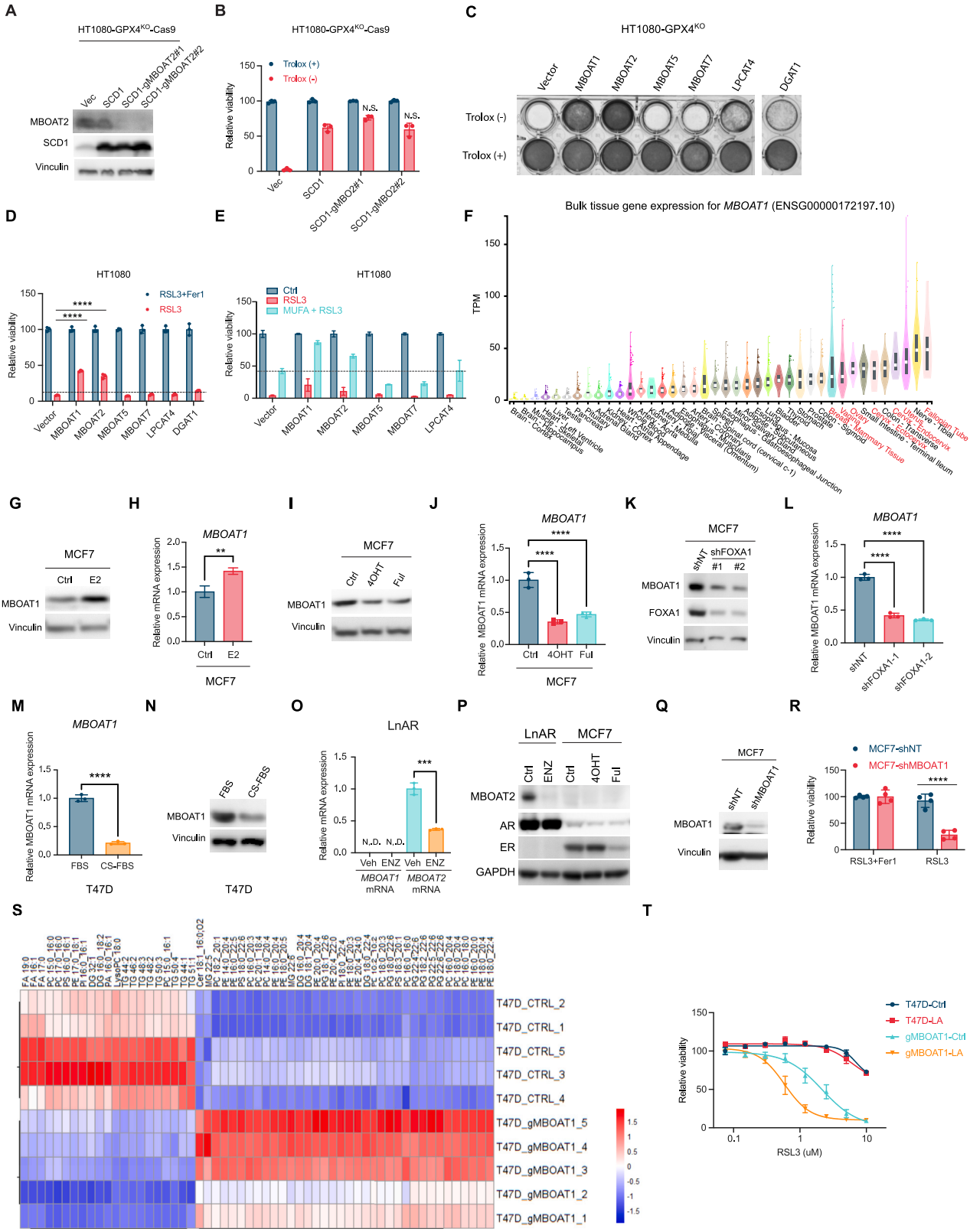

(legend on next page)

Figure S6. MBOAT1 suppresses ferroptosis and is regulated by ER signaling, related to Figure 6

(A) Western blot analysis showing expression of MBOAT2 and SCD1 in HT1080-GPX4^{KO} cells with SCD1 overexpression and/or MBOAT2 sgRNA knockout as indicated.

(B) Viability analysis of indicated cells cultured with or without 100 μM trolox for 24 h. Data are presented as mean ± SD (n = 3 biologically independent samples).

(C) Crystal violet staining of HT1080-GPX4^{KO} cells overexpressing indicated genes cultured with or without trolox for 72 h. Two independent experiments were performed, and representative images from one experiment are shown.

(D) Viability analysis of HT1080 cells overexpressing indicated genes. Ferroptosis was induced by 0.1 μM RSL3 for 24 h in the absence or presence of 10 μM Fer1 as indicated. Data are presented as mean ± SD (n = 3 biologically independent samples).

(E) Viability analysis of HT1080 cells overexpressing indicated genes. Cells were with or without MUFA pretreatment (10 μM OA) as indicated for 16 h, followed by ferroptosis induction with 1 μM RSL3 for 24 h. Data are presented as mean ± SD (n = 3 biologically independent samples).

(F) *MBOAT1* mRNA expression in normal human tissues (adapted from GTEx Portal) Expression levels are shown in TPM (transcripts per million). Boxplots are shown as median and 25th and 75th percentiles.

(G and H) MBOAT1 expression was detected by western blot (G) or qRT-PCR (H) in MCF7 cells that treated either with DMSO control (Ctrl) or 100 nM E2 for 48 h. Data are presented as mean ± SD (n = 3 biologically independent samples).

(I and J) MBOAT1 expression was detected by western blot (I) or qRT-PCR (J) in MCF7 cells that treated either with DMSO Ctrl, 1 μM 4OHT, or 0.5 μM fulvestrant (Ful) for 48 h. Data are presented as mean ± SD (n = 3 biologically independent samples).

(K and L) MBOAT1 and FOXA1 expression was detected by western blot (K) or qRT-PCR (L) in MCF7-shNT and MCF7-shFOXA1 cells. Data are presented as mean ± SD (n = 3 biologically independent samples).

(M and N) MBOAT1 expression was detected by qRT-PCR (M) or western blot (N) in T47D cells cultured with medium containing 10% FBS or CS-FBS for 48 h. Data are presented as mean ± SD (n = 3 biologically independent samples).

(O) qRT-PCR analysis showing *MBOAT1* and *MBOAT2* mRNA level in LnAR cells treated with DMSO vehicle control or 5 μM ENZ for 48 h. Data are presented as mean ± SD (n = 3 biologically independent samples).

(P) Western blot analysis showing MBOAT2, AR, and ER expression in LnAR and MCF7 cells subjecting indicated treatment for 48 h. ENZ: 5 μM; 4OHT: 10 μM; Ful: 0.5 μM.

(Q) Western blot analysis showing MBOAT1 expression in MCF7-shNT and MCF7-shMBOAT1 cells.

(R) Viability analysis of MCF7-shNT and MCF7-shMBOAT1 cells treated with 5 μM RSL3 for 24 h in the presence or absence of 10 μM Fer1 as indicated. Data are presented as mean ± SD (n = 4 biologically independent samples).

(S) Heatmap of lipid species that were significantly changed between T47D-Cas9 and T47D-gMBOAT1 cells. Two-tailed t test, FDR-corrected p value < 0.05, fold change threshold = 1.5.

(T) Viability analysis of T47D-Cas9 and T47D-gMBOAT1 cells treated with 10 μM LA for 24 h, followed with indicated concentration of RSL3 for 24 h. Data are presented as mean ± SD (n = 3 biologically independent samples).

Statistical analysis was performed using one-way ANOVA (B, D, J, and L) or two-tailed t test (H, M, O, and R). **p < 0.01, ***p < 0.001, ****p < 0.0001.

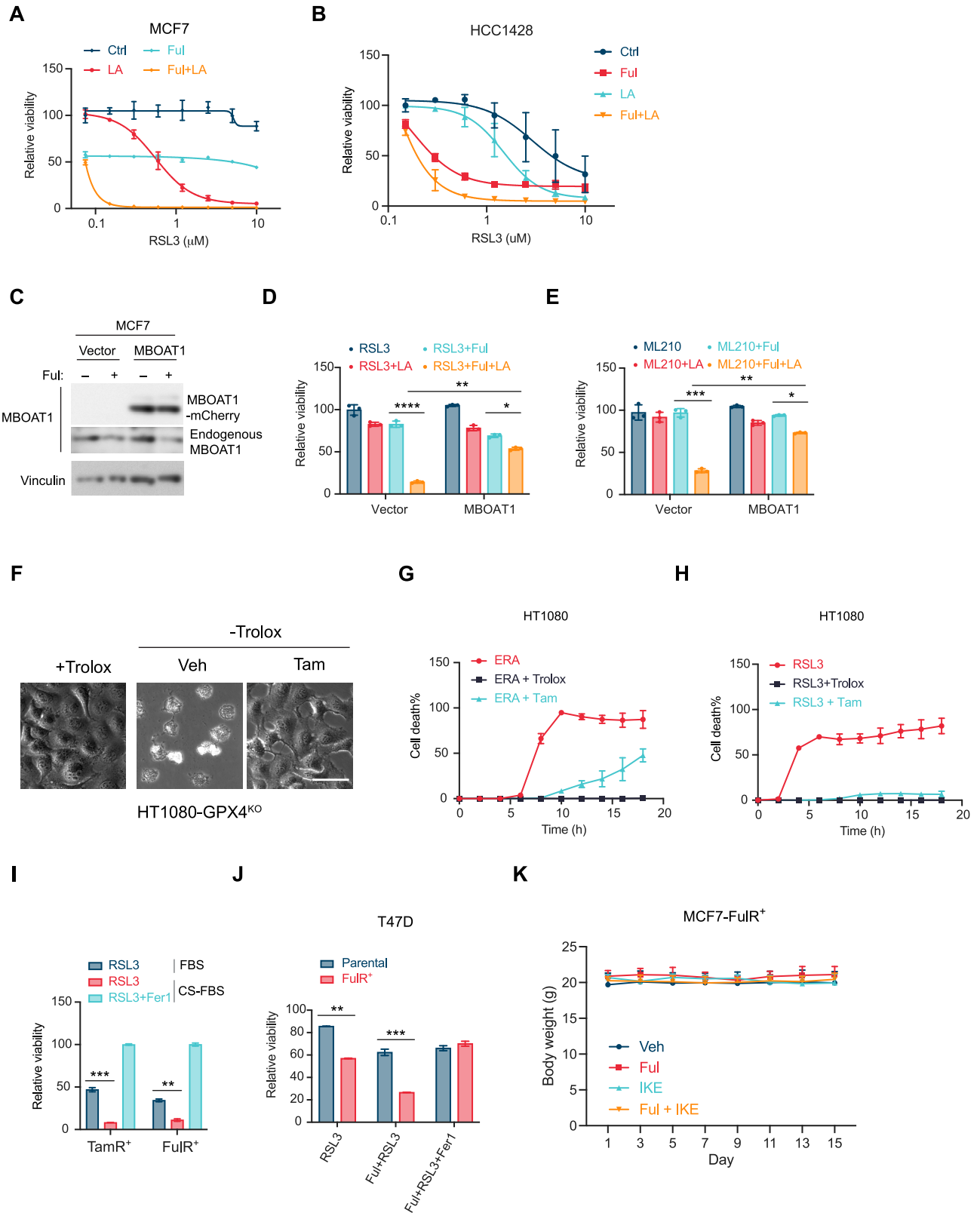

(legend on next page)

Figure S7. Fulvestrant sensitizes hormone therapy-resistant ER$^+$ breast cancer to ferroptosis, related to Figure 7

(A and B) Viability analysis of MCF7 (A) or HCC1428 (B) cells. As indicated, cells were pretreated with 0.5 μM Ful for 24 h, followed by incubation with 10 μM LA for 24 h. Subsequently, ferroptosis was induced with indicated concentration of RSL3 for 24 h. Data are presented as mean ± SD (n = 3 biologically independent samples).

(C) Western blot analysis showing expression of endogenous and ectopic MBOAT1 in MCF7-vector and MCF7-MBOAT1 cells treated with 0.5 μM fulvestrant as indicated for 48 h.

(D and E) Viability analysis of MCF7 cells harboring vector or MBOAT1 overexpression as indicated. Cells were pretreated with or without 0.5 μM fulvestrant (Ful) for 24 h, followed by incubation with 10 μM LA for 24 h. Subsequently, ferroptosis was induced by 1 μM RSL3 (D) or 1 μM ML210 (E) for 24 h. Data are presented as mean ± SD (n = 3 biologically independent samples).

(F) Images showing viability of HT1080-GPX4^{KO} cells with indicated treatment for 24 h. Trolox: 100 μM; Tam: 10 μM. Veh: DMSO as vehicle control. Two independent experiments were performed, and representative images from one experiment are shown. Scale bars, 20 μm.

(G and H) Cell death time course of HT1080 cells treated either with 0.2 μM erastin (G) or 0.1 μM RSL3 (H) with the supplement of 100 μM trolox or 10 μM 4OHT as indicated. Data are presented as mean ± SD (n = 3 biologically independent samples).

(I) Viability analysis of MCF7-TamR$^+$ and MCF7-FulR$^+$ cells cultured with 10% FBS or 10% CS-FBS for 48 h, followed by ferroptosis induction with 5 μM RSL3 for 24 h in the absence or presence of 10 μM Fer1 as indicated. Data are presented as mean ± SD (n = 3 biologically independent samples).

(J) Viability analysis of T47D-parental or T47D-FulR$^+$ cells. As indicated, cells were pretreated with or without 0.5 μM Ful for 48 h followed by ferroptosis induction with 5 μM RSL3 for another 24 h in the presence or absence of 10 μM Fer1. Data are presented as mean ± SD (n = 3 biologically independent samples).

(K) Body weight curve of mice from Figure 7K. Data are presented as mean ± SD (n = 5 or 6).

Statistical analysis was performed using one-way ANOVA (D, E, and I) or two-tailed t test (J). *$p < 0.05$, **$p < 0.01$, ***$p < 0.001$, ****$p < 0.0001$.